Revista
CIENCIA

Vol. **14, 2**, 215-249 (2011)

SOURCE COMPOSITION AND GEOCHEMICAL EVOLUTION OF SHALES FROM BARBERTON GREENSTONE BELT OF SOUTH AFRICA, BASED ON A MINERALOGICAL, GEOCHEMICAL AND ISOTOPIC INVESTIGATION

Theofilos Toulkeridis [(1)]*, Norbert Clauer [(2)], Alfred Kröner [(3)] and Wolfgang Todt [(4)]

(1) Center of Scientific Research (CEINCI), Geodynamic Division, Escuela Politécnica del Ejército (ESPE), P.O.Box 171-5-231-B, Sangolquí, Ecuador
(2) Centre de Géochimie de la Surface (CNRS/UdS), Université de Strasbourg, 67084 Strasbourg, France,
(3) Institut für Geowissenschaften, Universität Mainz, 55099 Mainz, Germany,
(4) Max Planck Institut für Chemie, Abteilung Geochemie, 55020 Mainz, Germany
* Corresponding author: Theofilos Toulkeridis, e-mail address: ttoulkeridis@espe.edu.ec or theousfq@yahoo.com

ABSTRACT

Major, trace and rare-earth elemental compositions as well as Rb-Sr, Sm-Nd and Pb-Pb isotopic systematics were determined on shales of the ~3.5-3.1 Ga old Barberton Greenstone Belt in South Africa to constrain their source compositions and evolution degree, on the basis of a their chemical alteration. A progressive change in the chemical composition has been identified in the sedimentary sequence from a dominant ultramafic-mafic (such as a komatiite end-member) source at the base of the sequence to a progressively felsic-plutonic (such as a granite end-member) source towards the top. The SiO2, K2O, U, Rb, Ba, Sr contents and the Zr/Y ratio increase proportionally upward, while the MgO, Fe2O3 contents and the Sm/Nd and Cr/Zr ratios consistently decrease. Both groups of rocks yield also high concentrations of Cr and Ni in comparison to shales of other Archaean occurrences.

The shales of the Fig Tree Group provide varied REE patterns with LaN/YbN ratios of 6.6±1.9 (2σ) and Eu/Eu* ratios of 0.86±0.11, while those of the Moodies Group yield more fractionated and scattered REE patterns with LaN/YbN ratios of 8.8±4.6, and similar Eu/Eu* ratios of 0.91±0.18, most being analytically not significant. The REE patterns of both sedimentary rock groups also outline slightly positive Eu-anomalies. An upward increase in the GdN/YbN, Th/Sc, La/Sc and La/Yb ratios, and a decrease in the Sm/Nd ratio, are also considered to reflect a change from a relatively undifferentiated mafic upper-crustal source to a more differentiated felsic composition.

The TDM Sm-Nd ages range between 3.02 and 3.85 Ga for the shales of both groups, indicating partly heterogeneous mantle sources, predominantly of either mafic rocks from lower Greenstone Belt itself, or of granitoïd rocks surrounding the belt. The Rb-Sr and Pb-Pb isotopic ages are at 2.6-2.7 Ga for the Fig Tree shales, while those of the Moodies Group are less constrained at about 2.2-2.3 Ga. These ages provide arguments for an alteration process caused by either a thermal or a chemical event that reset and/or, at least, disturbed the isotopic systems of the studied samples, resulting from large-scale fluid migrations. High ε_{Nd} values for the time of deposition probably reflect as well an open behavior of the Sm-Nd isotopic system.

Keywords.- Major, trace and rare-earth geochemistry, Rb-Sr, Sm-Nd and Pb-Pb isotopic systems, shales, Fig Tree and Moodies groups, Greenstone Belt, South Africa

1. INTRODUCCIÓN

Major, trace and rare-earth elemental (REE) compositions, in conjunction with isotopic systematic, such as the Rb-Sr, Sm-Nd and Pb-Pb methods, are increasingly used to constrain

Recibido: Marzo de 2011
Aceptado: Junio de 2011

provenance, source compositions, diagenetic evolution and weathering patterns of old sedimentary sequences. They also represent an original approach to identify ancient metamorphic episodes and tectonic evolutions of continents (e.g., McLennan 1982; Taylor and McLennan, 1985; McLennan et al., 1993; McDaniel et al., 1994; Hemming et al., 1995; Jahn and Condie, 1995). In fact, combined mineralogical, geochemical and isotopic studies are best suited to provide information on the chemical composition and age as well as on the crustal-to-sedimentary evolution of the source material of Archaean sedimentary rocks, especially of shales (Fedo et al., 1996; Hofmann et al., 2003).

In the present study, the mineralogical, elemental, and Sr, Nd and Pb isotopic compositions of early Archaean shales have been determined to contribute to an increased understanding of the evolution of the Barberton Greenstone Belt (BGB) of South Africa. The data presented were thought to complement the available information that has been reported previously on identical and similar rocks by McLennan et al. (1983b) and Hofmann (2005). They will be discussed in four different topics that appear quite appropriate for such old sediments: (1) the weathering effects in the source areas, (2) the origin and provenance of the detrital materials, (3) the possible hydraulic sorting of these detrital components, and (4) the impact of the tectonic-metamorphic setting in their evolution. It shall be added that Archaean sedimentary rocks are of special interest for this kind of investigation, because they are generally considered to represent the ultimate original sediments on Earth, not having been recycled through cannibalistic sedimentation processes.

In a previous study of sedimentary rocks from BGB, Hofmann (2005) concluded that chemical weathering of the source material that contributed to the whole 1200 m thick sedimentary sequence is minor, but that alternatively hydrothermal-metasomatic episodes affected the sequence significantly. He also reported varying contributions of ultramafic and mafic greenstones in the rock composition, depending on the studied rock facies. Since Hofmann's (2005) study was based on the varied rock lithologies of the Fig Tree Group, it appeared of interest to complement his study and contribute to the information about the source provenance and the chemical post-sedimentary evolution by detailing the mineralogical (whole rocks and mineral fractions), morphological (electron microscopy), geochemical (major, trace and rare-earth elements) and isotopic (Rb-Sr, Sm-Nd, Pb-Pb) aspects of the sole shale facies of the Fig Tree and Moodies groups, which we did in the present study.

2. GEOLOGICAL SETTING AND SAMPLING STRATEGY

The BGB is located near the southeastern edge of the Kaapvaal craton in southern Africa (Fig. 1); it consists of deformed and variably metamorphosed volcanic and sedimentary rocks of the Swaziland Supergroup (e.g., SACS, 1980). These supracrustal units are in intrusive or structural contact with the surrounding coeval or younger granitoïd plutons (Anhaeusser, 1973; Anhaeusser and Robb, 1981). The lower succession of the Swaziland Supergroup, which belongs to the 3.5-3.29 Ga old Onverwacht Group (Kröner and Todt, 1988; Armstrong et al., 1990; Lopez-Martinez et al., 1992), is 8-10 km thick and consists mainly of mafic and ultramafic rocks with minor sedimentary and felsic volcanic layers (Viljoen and Viljoen, 1969). It is overlain, apparently conformably, by a dominantly sedimentary sequence consisting in the Fig Tree (FTG) and Moodies (MG) groups. The 3.26-3.22 Ga old FTG (Kröner et al., 1991; Kamo and Davies, 1993) is 1-3 km thick and consists of a succession of greywackes, shales, cherts, dacitic flows and volcanics. The uppermost unit of the Swaziland Supergroup is the 3.22-3.1 Ga old MG, comprising up to 3.7 km of inter-bedded, compositionally immature to mature, dominantly quartzite sandstones, polymict conglomerates and subordinate siltstones, shales, and volcanics (Heubeck and Lowe, 1994a). Detailed stratigraphic studies also report a subdivision of the general stratigraphic succession into a northern, a west-central and a southern facies (Kröner et al., 1991; Lowe and Byerly, 1999) that are separated by the Inyoka fault (Fig. 1). In the northern zone of the BGB, the FTG and MG are considered to be in para-conformable contact suggesting the occurrence of a tectonic event (Eriksson et al., 1994).

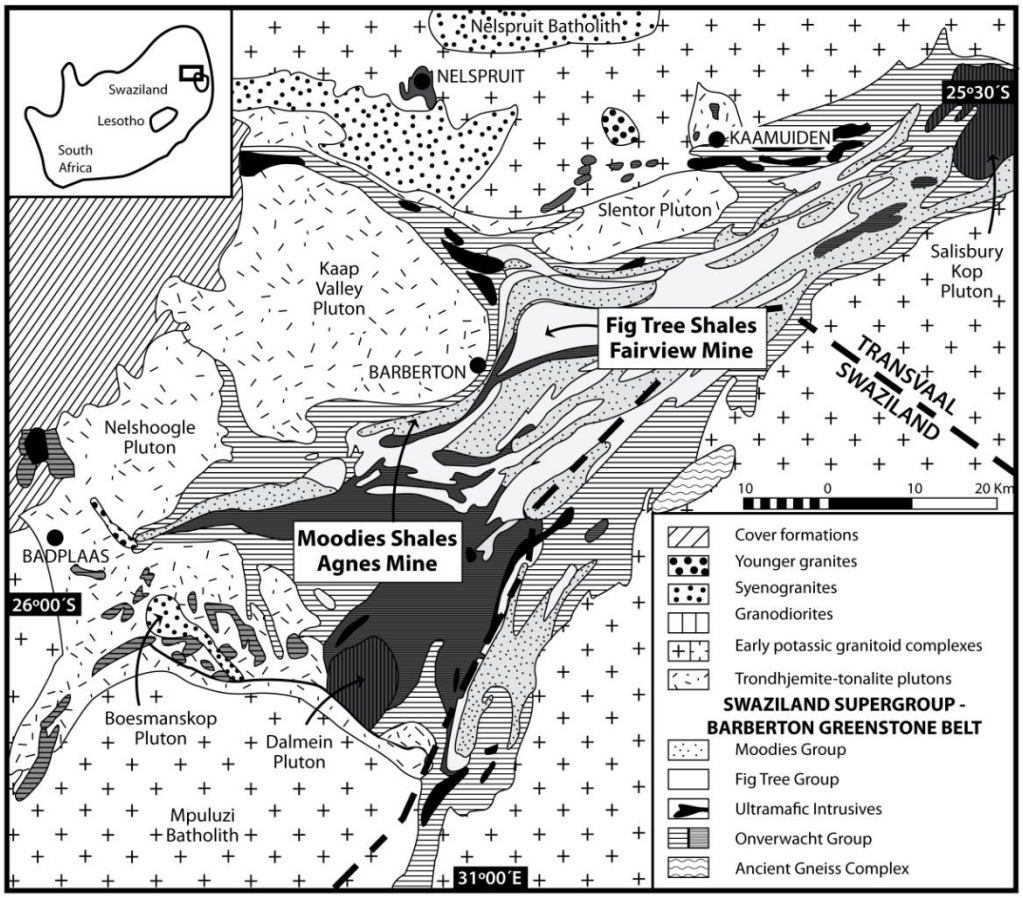

Figure 1: General geologic map of the Barberton greenstone belt with surrounding plutons.

Although all Barberton rocks have been virtually affected by a low-grade metasomatic alteration involving silicification, carbonatisation and widespread formation of secondary sericite and chlorite, they widely preserve primary volcanic and sedimentary lithologies, structures and textures (Nocita and Lowe, 1990; Lowe, 1991). Units within the belt were the subject of varied geochronological (e.g., Allsopp et al., 1973; Barton et al., 1983; Armstrong et al., 1990; Kröner et al., 1991), structural (Heubeck and Lowe, 1994a; De Ronde et al., 1994), metamorphic (Cloete, 1991) and sedimentological investigations (Erikkson et al., 1994; Lowe and Nocita, 1999). Major thermal events affected the belt after deposition of the Moodies Group at ~3.1, ~2.7 and ~2.1 Ga (Weis and Wasserburg, 1987; De Ronde et al, 1991; Toulkeridis et al., 1994; 1998).

Two sets of seventeen and nine samples were collected for the present study. The first consists of seventeen drill cores of shales from FTG that were taken near the Fairview Gold Mine. The second comprises nine drill cores from MG that were taken near the Agnes Gold Mine (Fig.1). Both can be considered to be fairly representative of the shale facies in the two groups.

3. ANALYTICAL PROCEDURE

Mineralogical data were obtained by X-Ray diffraction (XRD) and by optical and scanning electron-microscope (SEM) observations (Table 1). The SEM was equipped with an EDX system for chemical analysis of polished thin-sections and whole-rock chips. Additional information including the chemical composition of the clay fraction is available in Toulkeridis et al. (1996).

The selected drill cores were ~20-25 cm in length and ~4 cm in diameter; they were first cleaned for any visible weathering feature or any vein occurrence. Then, they were crushed into 2-4 mm chips, rinsed several times with distilled water and pulverized in a disc mill. The major and some trace elements were determined by XRF (Phillips PW 1404) following a description of Stern (1972) and by ICP-AE (ARL 35000). The additional trace and REE were measured by ICP-MS (Fison VG Isoplasma) following the procedure of Samuel et al. (1985) also valid for the ICP-AE measurements. Replicate analyses of reference samples and standards indicate that the accuracy of the major elements was within ±5% and that of the trace- and REE determinations within ±10%. This analytical accuracy means that if the REE contents of the samples, as well as their Ce and Eu anomalies, range between 0.9 and 1.1 relative to those of any reference, they are not analytically significant. All REE data were normalized for plots using the chondrite values of Taylor and McLennan (1985) as the reference material. Elemental contents and some selected ratios of the samples are given in the Tables 2, 3 and 4.

The Rb-Sr isotopic analyses were performed on a VG Sector multi-collector mass spectrometer at the Centre de Géochimie de la Surface of Strasbourg. The samples were dissolved in teflon containers in Mainz with a triacid ($HF + HNO_3 + HClO_4$) mixture. The Sr, Sm and Nd were separated in Strasbourg using a chemical procedure similar to that reported by Schaltegger et al. (1994). The value obtained for the NBS 987 standard during the course of the study was 87Sr/86Sr = 0.710257±0.000015 (2σ external, n = 4). For the isochron calculation, a systematic uncertainty of 0.000015 (2σ) was taken for each measured $^{87}Sr/^{86}Sr$ ratio on the basis of the standard reproducibility. The accuracy of the $^{87}Rb/^{86}Sr$ ratio was better than 1.5%. All $^{87}Sr/^{86}Sr$ ratios were corrected to the NBS 987 standard $^{86}Sr/^{88}Sr$ ratio of 0.1194 (Table 4).

The Sm-Nd isotopic analyses were obtained on two Finnigan MAT 261 mass-spectrometers at the Max-Planck Institut für Chemie in Mainz. The $^{143}Nd/^{144}Nd$ ratios were normalized to a $^{146}Nd/^{144}Nd$ ratio of 0.7219. The value obtained for La Jolla Nd standard was $^{143}Nd/^{144}Nd$ = 0.511843±0.000020 (2σ external, n = 11) during this study. For isochron calculation, a systematic uncertainty of 0.000020 (2σ) was assumed for the measured $^{143}Nd/^{144}Nd$ ratio on the basis of reproducibility of the standard. When the specific measurement error of a given analysis was higher than 0.000020 (2σ), the higher value was used. The uncertainty for the $^{147}Sm/^{144}Nd$ ratio was taken as 0.2%. All $^{143}Nd/^{144}Nd$ ratios were corrected to the La Jolla standard $^{143}Nd/^{144}Nd$ ratio of 0.511860 (Table 4).

The Pb isotopic ratios were determined in static mode on a Finnigan MAT-261 mass-spectrometer at the Max-Planck-Institut für Chemie in Mainz. Pb was purified following a standard ion exchange technique (Krogh, 1973), and was measured on single Re filaments with a mixture of phosphoric acid and Si-gel (Cameron et al., 1969). The Pb isotopes were then individually measured, and the isotopic ratios were corrected for a mass fractionation factor of 0.1% per amu determined by measurements of the NBS 982 standard. When the specific measurement error of an analysis was higher than the error value defined by the 2σ of the NBS 982, the higher value was used (Table 4).

4. RESULTS

4.1. Mineralogy

The FTG and MG shales consist mainly of quartz, illite, chlorite and albite. Monazite (rhabdophane), apatite, Cr-spinel, zircon, sphene, which might be of authigenic origin (Morad and Aldahan, 1985; 1986; Panhuys-Sigler and Trewin, 1990), and diverse heavy minerals including sulfides and oxides represent the minor constituents (Fig. 2A to L). The illite content of the <2μm fraction of the FTG shales varies between 10 to 45%, averaging 17% with the remainder being chlorite. The MG shales contain up to 100% illite with an average of 86%, and small amounts of chlorite. Both Fe- and Mg-rich chlorites are present; the Mg-rich being dominant in the MG shales (Toulkeridis et al., 1996). Two samples yield a significantly different mineral composition than the others: sample 79NC127 collected close to the magnetite shale

contains ~30 % magnetite, and sample 79NC107 is extensively silicified. Some of the samples were found to be crosscut by thin (0.5µm-1mm) veins of dolomite, quartz, gold, sphalerite or pyrite (Table 1). It might also be mentioned that the analyzed rocks were not subjected to a metamorphic degree higher than incipient greenschist facies.

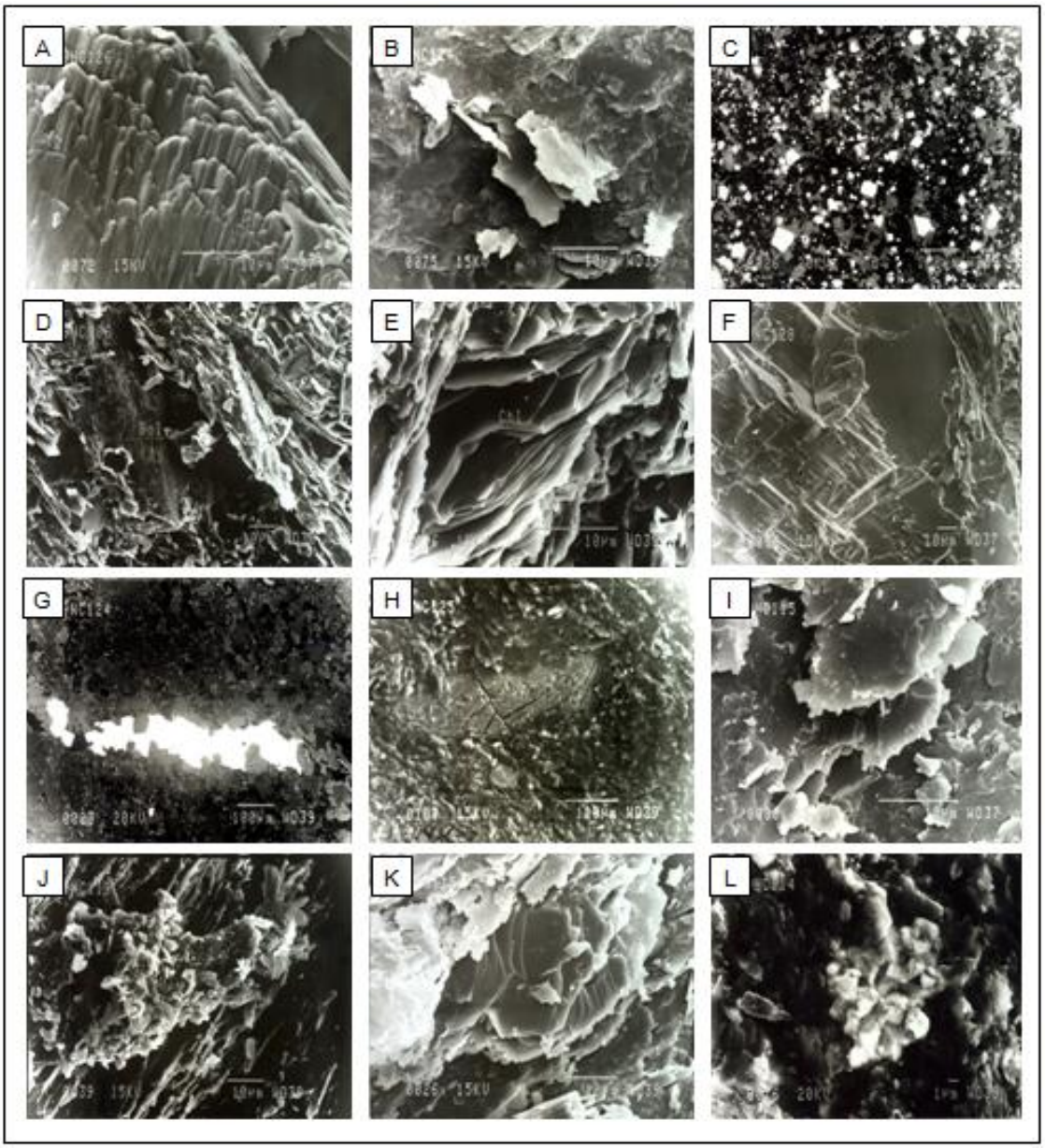

Figure 2: Pictures by Scanning Electron Microscopy of some minerals characteristic of the FTG shales (from A to F) and of the MG shales (G to L)

4.2. Major-elemental geochemistry

Chemical variations relative to the stratigraphic position of the samples are obvious in the composition of the major elements. Except for the two specific samples 79NC107 (FTG shale) and 79NC127 (MG shale) that were identified by the XRD analysis, the SiO_2 contents of the FTG shales range from 50.2 to 58.9 weight percent (wt%) with an average of 54.4 wt%. They are lower than those of the SiO_2 in the MG shales, ranging from 55.5 to 63.1 wt% with an average at 60.4 wt%. The FTG shales contain higher TiO_2, Fe_2O_3*, MnO, MgO, P_2O_5, (LOI) contents, and lower K_2O and Na_2O contents than the MG shales.

Relative to the North American Shale Composites (NASC; Gromet et al., 1984), both the FTG and the MG shales yield lower SiO_2, TiO_2 and CaO contents and almost identical Al_2O_3, Na_2O and P_2O_5 contents; the MgO and MnO contents being higher. The FTG shales contain more Fe_2O_3 and the MG shales less than the NASC, whereas the K_2O contents correlate negatively with those of the NASC. The FTG shales yield slightly lower K_2O/Na_2O ratios but of a wider scatter than the MG shales, both averaging lower K_2O/Na_2O ratios than the NASC, but exceeding slightly the known range of this ratio in shales of other greenstone belts, which is between 0.7 and 1.5 (Taylor et al., 1986; Wronkiewicz and Condie, 1989). The SiO_2/Al_2O_3 ratio of the FTG shales is slightly lower than that of the MG shales, ranging within the known variation of Archaean greenstone shales (from ~3 to ~5). Besides some shales of the Pongola Supergroup, most of the MG shales outline higher K_2O contents than Archaean and early Proterozoic shales of the Kaapvaal Craton (Wronkiewicz and Condie, 1990; Eriksson et al., 1990).

For identification of the main Al-bearing components of the shales, the TiO_2, Fe_2O_3 and K_2O contents were plotted relative to the Al_2O_3 contents. The FTG and MG samples show obvious differences. For instance, the TiO_2 content correlates positively with the Al_2O_3 content (Fig. 3A), but all samples plot above the assumed field of the clay minerals (Veizer, 1978; Veizer and Garret, 1978), which corroborates the assumption that heavy minerals, such as titanite and illmenite, are the main carriers of Ti and are intimately mixed with the clay particles in the <2µm fraction.

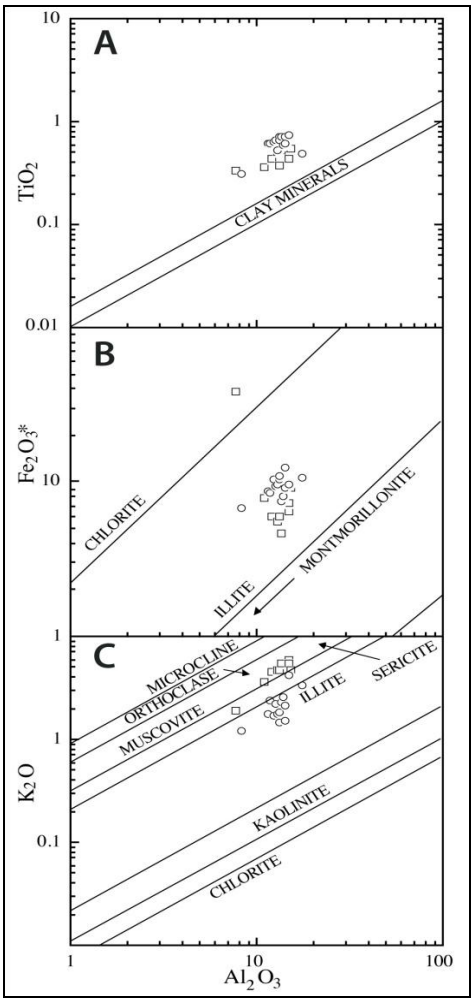

Figure 3: Logarithmic plots of TiO2 (in A), Fe2O3 (in B) and K2O (in C) vs. Al2O3. All contents are in wt%.

Considering that clay minerals are the main carriers of Fe and K as well, can help to differentiate distinctive fields of clay minerals. In this respect, the FTG shales should contain clay material mainly chloritic in composition (Fig. 3B), whereas the MG shales should contain mixed-layered illite/smectite clays, which is not what the XRD study outlines, at least for the FTG shales. Alternatively, the field of the FTG shales close to the illite field, and the field of the MG shales close to a muscovite/sericite end member (Fig. 3C), both suggest that the mica-type minerals of the latter appear to have crystallized at higher temperatures, which again does not perfectly fit the XRD data mentioning the occurrence in these rocks of a mixed-layer illite/smectite that basically contains less K than illite.

Two sub-parallel linear trends are obtained in a K_2O-Fe_2O_3-Al_2O_3 ternary plot (Fig. 4). Trend A consists of the FTG shales, defining a tightly oriented cluster close to a komatiitic - basaltic composition. These shales are also enriched in Al_2O_3, confirming the mixing of illite and chlorite. Trend B is made up of MG shales that contain less Al_2O_3, with a narrow scatter along a mixing line defined by the chlorite and muscovite (perhaps mixed with minor K-feldspar) end-members. The anomalous sample 79NC127 plots close to the Fe_2O_3 corner, resulting from already mentioned high magnetite content. None of the shales plots in the field of residual clays (Reimer, 1985), implying no significant impact of modern weathering effects.

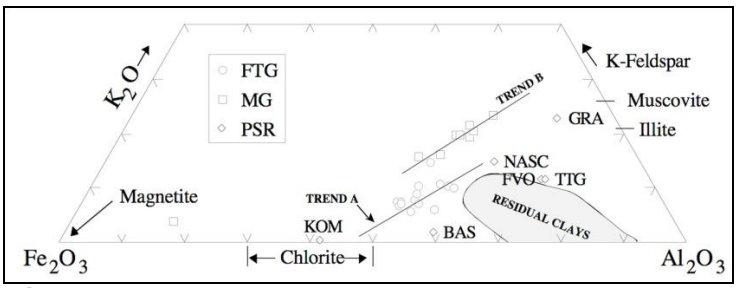

Figure 4: K_2O-Fe_2O_3-Al_2O_3 ternary plot adapted from Wronkiewicz and Condie (1987). Field of residual clays is from Reimer (1985).

Weathering of igneous rocks induces depletion of alkali- and alkaline-earth elements and preferential enrichment of Al_2O_3 in the resulting materials, thus providing a way of examining the sedimentary history of a bedded sequence. Weathering effects can be explained in terms of the Chemical Index of Weathering (CIW; Harnois, 1984) or the Chemical Index of Alteration (CIA; Nesbitt and Young, 1982). Changes in the CIW/CIA ratio of two different rock series may reflect changes in the mineral composition, which is not necessarily related to rock weathering and/or alteration, but to a transport sorting from source area to deposition site. The CIW index is defined as the $Al_2O_3/(Al_2O_3+CaO^*+Na_2O)$ ratio, while the CIA index results from $Al_2O_3/(Al_2O_3+CaO^*+Na_2O+K_2O)$ ratio, with CaO* including only Ca associated with silicate minerals (Nesbitt and Young, 1984; all oxides being in %mol). In the present study, CaO* was calculated by subtracting the contribution of apatite estimated from P_2O_5 content, and the amount of monazite and carbonate estimated from CaO-CO_2 calculation. The CIA values of the FTG shales average 64.1±9.8 (1σ) and those of the MG shales 56.5±3.3 (1σ), whereas the CIW values are at 78.5±7.5 for the FTG shales and 76.6±5.8 for the MG shales. The CIW and CIA trends ranging from 77 to 79 and from 56 to 64, respectively, are indicative of a lower weathering degree than in the reference shales (CIA = 70-75; Taylor and McLennan, 1985), reporting no determining weathering of the source components. Relative to the scatters obtained here, the CIA values of the average upper-continental crust are at about 50, that of muscovite at 75, and those of chlorite at 100 (Nesbitt and Young, 1989).

The CIA data of both groups of shales were also plotted in a ternary diagram of molar fractions of Al_2O_3, (CaO^*+Na_2O) and K_2O. Typical pristine igneous rocks plot below 50% of Al_2O_3, and the fluids associated with their alteration reflect preferential depletion of alkali/alkaline earths, plotting at or near 0% Al_2O_3 (Fig. 5). Shale compositions of both the FTG and MG cannot be explained simply by a removal of alkali/alkaline earths during weathering of a homogeneous source. If so, the line drawn through the data would display the composition of

the surface water associated with the weathering profile and would yield 0% Al_2O_3. The relative contents of Al_2O_3 in the FTG shales are almost identical, or even higher, than those of typical igneous compositions. They are also close to the NASC value, suggesting again that the source may have had a minor weathering history. The shales of both the FTG and MG define individual trends, which intersect the Al_2O_3, (CaO^*+Na_2O) tie line, showing that the chemical composition does not simply result from a weathering process. These trends may record chemical changes that occurred in the shales between weathering of the source rocks, deposition and final consolidation during compaction, including chemical alteration of detrital igneous minerals into clay components.

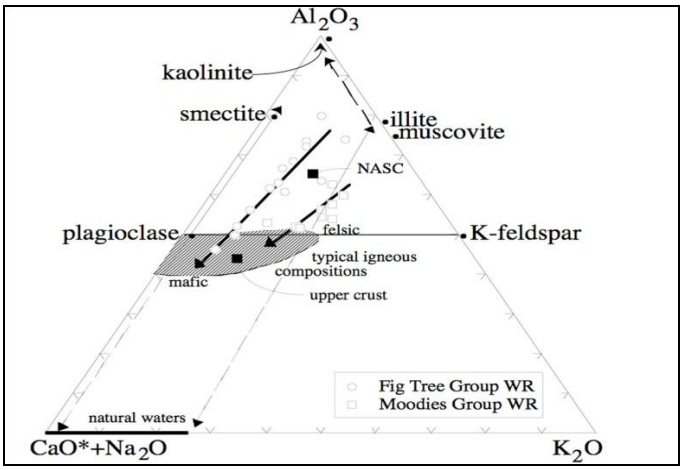

Figure 5: Ternary diagram of molar fractions of Al2O3-(CaO*+Na2O)-K2O.

In summary, the mineral composition of the studied shales is rather common with quartz, illite, chlorite, albite and minor heavy minerals. The rocks appear to have been subjected to an incipient greenschist metamorphic degree, with the MG shales apparently more recrystallized. Also, it might be mentioned that only very insignificant weathering effects, either ancien or recent, were detected.

4.3. Large-ion lithophile elemental (LILE), rare-earth elemental (REE) geochemistry

The FTG shales contain lower Rb, Sr, Cs, U and Th contents than the MG shales and the NASC reference. The Rb, Sr, Ba and Cs concentrations are half those of the MG shales, which have lower contents in Sr, U, Ba and Th, but higher contents in Cs and Rb than the NASC. The Th/U and K/Rb ratios of the MG shales are generally higher than those of the NASC, while those of the FTG shales are lower. Both, the FTG and MG shales yield lower Th/Sc ratios, but higher Rb/Sr and Ba/Sr ratios than the NASC.

In plotting Rb against K and in assuming that both are in the illite mineral phase, a differentiation between detrital and authigenic illite can be made (Fig. 6). In the present case, the FTG shales seem to contain predominantly detrital illite, whereas the MG shales seem to contain mainly authigenic illite, which confirms an earlier trend on the recrystallization degree of the rocks.

The REEs are known to be reliable provenance indicators (e.g., Taylor and McLennan, 1985), because they tend to be transferred non-fractionated from source material to the sedimentary site, therefore reflecting the average REE composition of the source (Cullers et al., 1979; McLennan et al., 1980). Although this assumption seems not to be shared by all (Chaudhuri et al., 1992; Honty et al., 2008) and although the absolute concentrations in REEs are variable, chondrite-normalized patterns are almost similar for both groups with steep patterns typical for Archaean clastic sedimentary rocks providing La_N/Yb_N ratios of 6.6 for the FTG shales and of 8.8 for the MG shales (Fig. 7). Light REEs (LREE) contents are 35 to 100

times those of the average La_N/Sm_N ratios of chondrites, and those of the heavy REEs (HREE) are 5 to 15 times those of the chondrites. The patterns of the HREEs are relatively flat for both groups with Gd_N/Yb_N ratios of ~1.4 that fall into a 1-to-2 value range typical for Archaean sedimentary rocks (McLennan, 1989). The Eu/Eu* anomaly, which describes the enrichment of Eu relative to a smooth pattern with Eu* being the geometric average value between Sm_N and Gd_N (i.e. $\frac{Eu}{Eu^*} = \frac{Eu_N}{\sqrt{Sm_N * Gd_N}}$), is negative in almost all FTG and MG shales, as already reported in other Archean sedimentary rocks (Gao and Wedepohl, 1995). It ranges from slightly positive to negative in the MG shales, while being consistently slightly negative in the FTG shales. Similarly, the Ce/Ce* ratio $\frac{Ce}{Ce^*} = \frac{Ce_N}{La_N^{\frac{2}{3}} * Nd_N^{\frac{1}{3}}}$ refers to the enrichment of Ce relative to a smooth distribution. Here, with values of ~0.98 for the MG shales and ~0.94 for the FTG shales this ratio shows no fractionation at all if considering the analytical uncertainty, while some negative values were obtained in other Barberton sedimentary rocks (Hayashi et al., 2004). Both the FTG and the MG shales yield the highest Eu/Eu* and Ce/Ce* anomalies when compared to NASC and to younger shales from Kaapvaal craton (e.g., Wronckiewicz and Condie, 1990; Jahn and Condie, 1995).

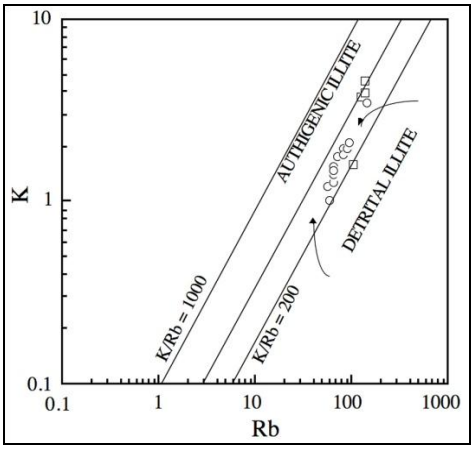

Figure 6: Logarithmic plot of Rb vs. K concentrations of the FTG and MG shales.

In summary, the K and Rb contents provide information about detrital and authigenic origin of the illite-type components in the FTG and MG shales, respectively. The REE contents are highly enriched relative to chondrites, and the Eu and Ce anomalies are limited or even absent.

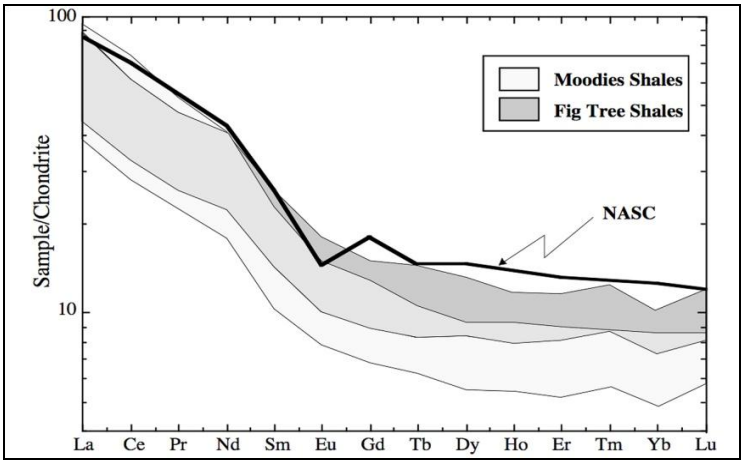

Figure 7: Chondrite-normalized REE patterns of the FTG and MG shales as well as of the NASC reference.

4.4. High-field strength elements (HFSEs) and transition-metallic elements geochemistry

Both, the FTG and MG shales yield lower Hf, Zr, Nb, Ta, Y and TiO2 contents than the NASC reference. Compared to the MG shales, the FTG shales contain less Ta, Nb, Zr and Hf, but more Y and TiO_2. They also have lower Zr/Y and higher Ti/Zr ratios, whereas the Zr/Nb ratios are almost the same in the FTG, the MG shales and the NASC. The TiO_2 and Y contents are negatively correlated, whereas all other HFSEs are scattered when plotted relative to the SiO_2 content, suggesting a distinctive mineral control. The Ti and Nb contents correlate positively in both groups, indicating the occurrence of ilmenite as the main hosting mineral. The average Zr/Hf ratios are slightly higher in the MG shales (~33) than in the FTG shales (~30). Although the Zr/Hf ratio ranges from about 23 to 45 in the MG shales, most samples yield values between 38 and 45, suggesting a zircon control (Zr/Hf ≈ 40) for these elements. While most FTG shales have Zr/Hf ratios below ~30, it appears that Hf is controlled by, at least, one additional mineral. The HREEs, LREEs, Th, U and Y concentrations of the MG shales are positively correlated with Zr, suggesting that they are carried dominantly by zircon. The Th, U and Y contents of the FTG shales also correlate positively with the Zr contents. The lack of correlation between the HREE and LREE and Zr indicates also that these elements are not hosted only by zircon.

Abnormally high abundances of Cr and Ni in FTG shales were first reported by Danchin (1967) and later by McLennan et al. (1983a) (Fig. 8A). Here, the Cr and Ni contents range from 850 to 1120 µg/g, and from 310 to 550 µg/g, respectively, with the exception of sample 79NC107 depleted in both Cr and Ni (390 µg/g, 190 µg/g), due to a dilution effect by extensive silicification. In comparison, the MG shales contain less Cr and Ni, between 510 and 850 µg/g, and 130 and 390 µg/g, respectively. Although the absolute abundances differ, the Cr/Ni ratio of both groups is similar at ~2.47, which is higher than that of komatiites (~1.6), which suggests a significant fractionation (Condie, 1993; Garver et al., 1996). A positive correlation exists between Cr, Ni and MgO, Sc and V for both groups of samples; all these elements being negatively correlated with SiO_2. The presence of Cr-spinel in the MG shales is often observed, whereas this Cr-carrying mineral has not been identified in the FTG shales. Typical Ni-carriers such as FeNiS and AsCoFeNiS were detected in both groups (Table 1). The Barberton shales show a 500 to 1000 % enrichment of Cr and Ni relative to NASC. Compared to other Archaean to Proterozoic shales from South Africa as well as to Archaean occurrences elsewhere in the world, the FTG shales yield the highest abundances in Cr and Ni (Fig. 8B). The Co content is highly variable in the MG shales relative to FTG shales, but both outline the same average amounts. The FTG shales are enriched in Sc, V and Co, whereas the MG shales contain similar amounts of Sc, lower amounts of V and higher amounts of Co, relative to NASC.

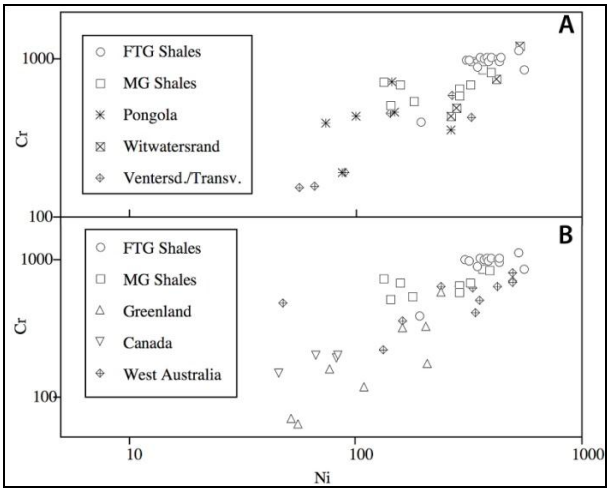

Figure 8: Logarithmic plot of Cr vs. Ni concentrations of the FTG and MG shales relative to other Archaean shales of South Africa (in A) and to other early Archaean occurrences (in B).

In summary, the HFSEs and metal elements confirm the occurrence of accessory heavy minerals that carry the REEs, Ta, Nb and Zr; Cr and Ni being mainly in Cr-spinel and sulfides.

5. DISCUSSION

The aim of the present study was a mineralogical, elemental and isotopic evaluation of at least the effects of: (1) weathering of the source area(s), (2) diagenetic and metamorphic alteration, (3) hydraulic sorting, as well as an identification of the provenance of the supplying material. These topics will be discussed hereunder.

5.1. Effects of hydraulic sorting, adsorption, diagenesis and metamorphism

Several petrographic studies including the evaluation of textural maturity, the characteristics of grain size and shape, and the mineral composition (Folk, 1974), which usually allow identification and evaluation of the sorting processes in sedimentary rocks, fail in fine-grained shale-type rocks (McLennan, 1989). For such rocks, the evaluation of the hydraulic sorting can be based on the chemical composition (McLennan et al., 1993). The presence of weathering-resistant zircon, Cr-spinel, magnetite, monazite and apatite may produce irregular chemical variations in some trace elements such as the REEs and the HFSEs (Gromet et al., 1984; Reimer, 1985; Cullers et al., 1979; Maas and McCulloch, 1991). When plotting the Th/Sc ratio vs. the Zr/Sc ratio, evaluation of the causes for zircon enrichment should be possible, as Zr is usually strongly enriched in zircon, while Sc is not but is generally able to preserve the signature of the provenance, as do the REEs (McLennan, 1989). The Th/Sc ratio appears, therefore, as a good indicator of igneous chemical differentiation processes, since Th is an incompatible and Sc a compatible element in igneous systems. Both, the Th/Sc and Zr/Sc ratios vary sympathetically in the FTG and the MG shales (Fig. 9), by following a trend that is consistent with a process primarily controlled by igneous differentiation (McLennan et al., 1993).

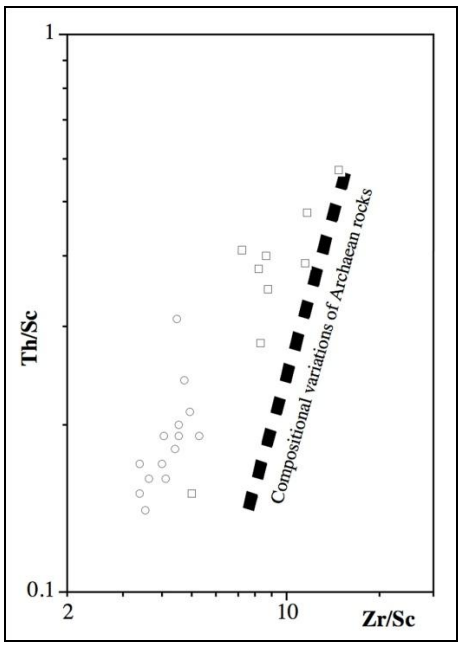

Figure 9: Plot of Th/Sc vs. Zr/Sc ratios of the FTG and MG shales.

Sedimentary sorting becomes detectable when Cr contents are plotted against Zr contents (Fig. 10). Here, the FTG shales form a tight cluster, while the MG shales are positively correlated, suggesting an accumulation caused by grain-size effect. This fact, combined with mineralogical observations, suggests that Cr may be adsorbed as promoted by Manceau and Calas (1986) onto the clay minerals of the FTG shales, while Cr appears to be mainly hosted in

Cr-spinel of the MG shales. A plot of the Gd_N/Yb_N ratio against the La_N/Sm_N ratio, in which "N" indicates chondrite-normalized values, shows a scatter for the FTG shales having La_N/Sm_N ratios between 2.6 and 3.7 and Gd_N/Yb_N ratios between 1.1 and 1.5 (Fig. 11), whereas the MG shales have La_N/Sm_N ratios from 3.5 to 4.8 and Gd_N/Yb_N ratios from 1.2 to 1.8. These scatters are not surprising given the potentially complex sorting of heavy minerals.

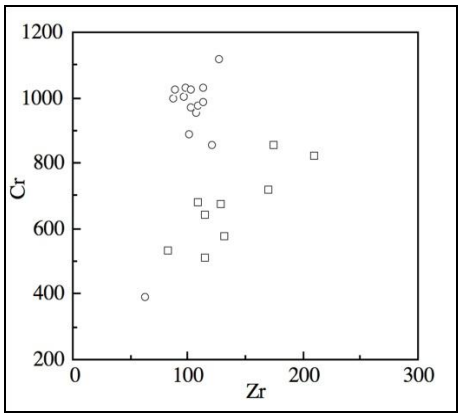

Figure 10: Plot of Cr vs. Zr contents of the FTG (circles) and MG (squares) shales.

Positive correlations between P_2O_5 contents and La and Ce contents suggest that apatite and monazite may also control the high amounts of LREEs. A positive correlation between Al_2O_3 and REEs suggests that the REEs belong mainly to Al-silicate minerals, probably of the clay type. Although clay minerals preferentially tend to adsorb REEs and metals from seawater (Roaldset, 1973; Balistieri and Murray, 1984), the resultant enrichment in these elements appears fairly uniform within the shale units during both deposition and diagenesis (Wronkiewicz and Condie, 1987). Similar REE distributions in each of the two groups suggest that if adsorption was important or at least dominant, it acted similarly for all the shales. Furthermore, the overall similarity of the REE patterns of the Barberton shales with those estimated for the average upper-Archaean crust (Taylor and McLennan, 1985; Condie, 1993) suggests that fractionation of the REEs is not a major factor that could have obscured the provenance compositions of the rocks (Wronkiewicz and Condie, 1987). Diagenesis and low-grade metamorphism, such as those affecting the Barberton shales studied here, generally produce only small changes, if any, in both the major and trace element concentrations of shale-type rocks (Cullers et al., 1974; Condie and Martell, 1983; Gromet et al., 1984; Schieber, 1988; Eriksson et al., 1990; Bierlein, 1995).

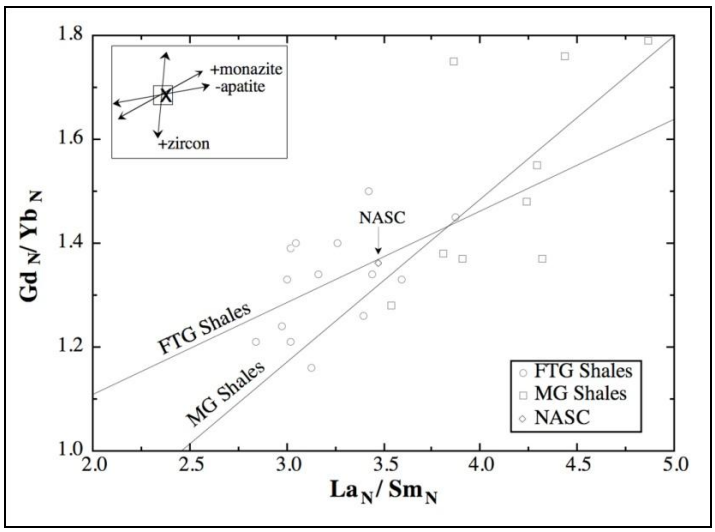

Figure 11: Plot of Gd_N/Yb_N vs. La_N/Sm_N ratios. NASC ratios are for reference.

5.2. Shale provenance

As already stated, shales are the most suitable sediments for provenance studies based on geochemical data, due to their homogeneity and post-depositional low permeability (Schieber, 1988; Wronkiewicz and Condie, 1989; Crighton and Condie, 1993), which reduces fluid migration and interaction with the host minerals. The FTG and MG shales most probably derived from source areas comprising either basaltic and komatiitic rocks from within the greenstone belt, or granitoïd rocks from around the Greenstone Belt. The presence of intercalated felsic volcanic rocks within the FTG indicates the further possibility of pene-contemporaneous felsic volcanic activity providing fine detritus to both the FTG and MG shale depositories.

While many factors such as hydraulic sorting and metamorphic imprint affect the composition of fine-grained terrigenous sediments, like those studied here, a robust and reliable provenance indicator is given by the triangular projections La-Th-Sc and Th-Hf-Co (Fig. 12; Wronkiewicz and Condie, 1987), as these elements (REEs, HFSEs, Th and Sc) are among the least mobile under an extensive range of geologic conditions. They represent, therefore, best candidates for provenance studies (Taylor and McLennan, 1985; Wronkiewicz and Condie, 1987). In addition, the La/Th fractionation is a good indicator of a felsic source composition, because these elements are mostly associated with quartz and are strongly controlled by the nature of the source rocks.

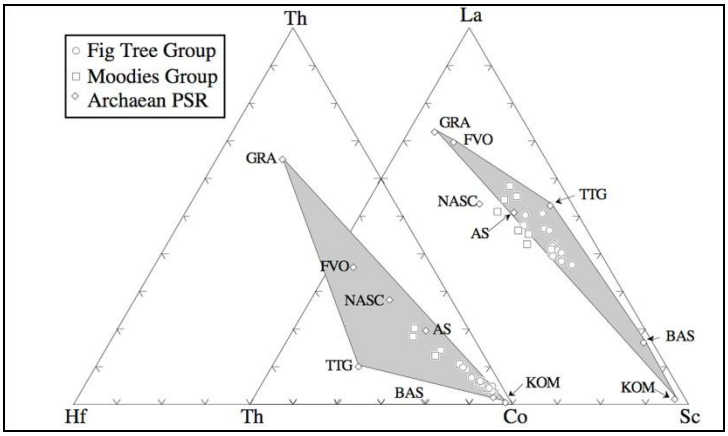

Figure 12: Double ternary diagram of Th-Hf-Co and La-Th-Sc contents, after Wronckiewicz and Condie (1987).

Alternatively, Sc and Co are more likely associated with a mafic source composition, providing a good antagonistic supply in the differentiation of the source of the shales. Also, the Th/Sc ratio is a sensitive index for provenance compositions (Taylor and McLennan, 1985; McLennan, 1989). In both diagrams, all shale data points plot in a field comprising all possible source rocks, which implies that the sources have been bimodal, i.e. mixed felsic-mafic in different proportions. The FTG shales are more mafic-related and the MG shales are more felsic-related (Fig. 12). The record of mixed sources as the provenance of shales in the geochemical data can also be observed on plots of Th/Sc vs. Th/Al_2O_3 ratios (Fig. 13A), Th/Al_2O_3 vs. Sc/Al_2O_3 ratios (Fig. 13B), or La/Al_2O_3 and La/Sc vs. La_N/Yb_N ratios (Fig. 13C,13D).

More specifically, the differentiation of FTG and MG shales can also be tested using diagrams of Zr and SiO_2 contents vs. Ti/Nb; Bonjour and Dabard (1991) having shown that the Ti/Nb ratios can be used as indicators of provenance for clastic terrigenous sediments. In Fig. 14A and Fig. 14B, the FTG shales have higher Ti/Nb ratios, but lower SiO_2 and Zr values, than the MG shales, thus confirming the above mentioned assumption of their source origin.

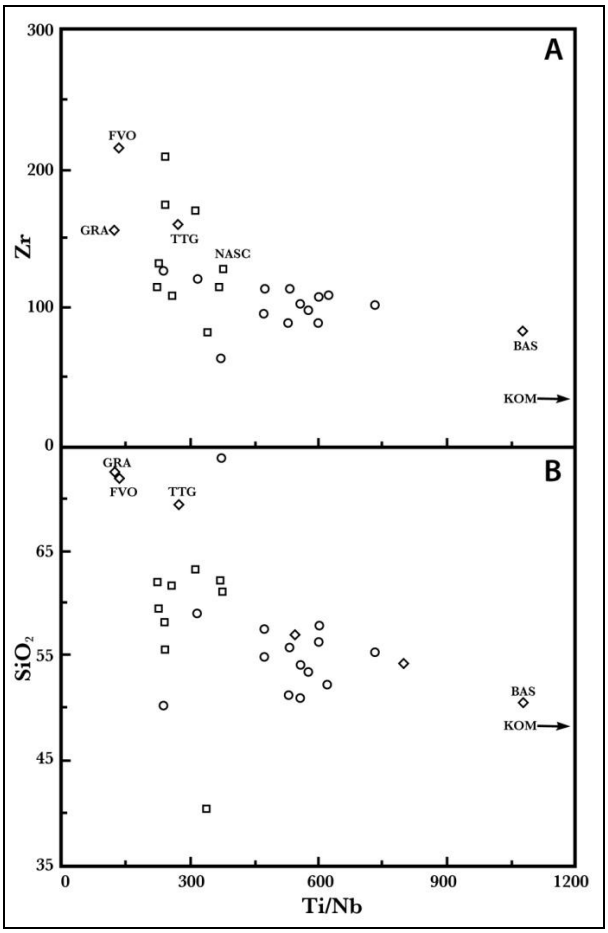

Figure 13: Plot of Zr contents vs. Ti/Nb ratios (in A), and SiO_2 contents vs. Ti/Nb ratios (in B).

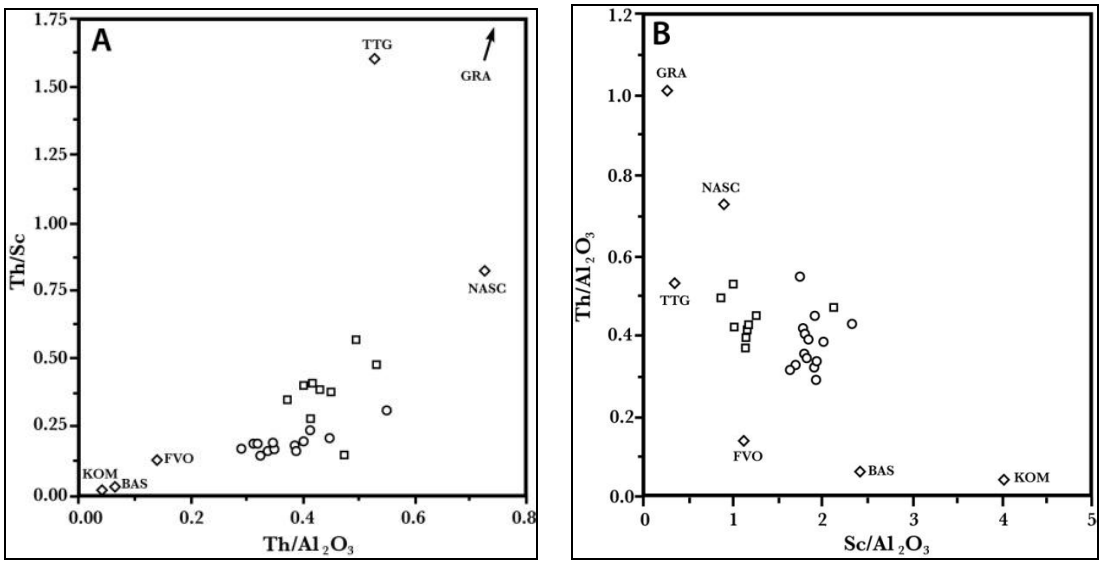

Figure 14 A-B: Plots of Th/Sc vs. Th/Al_2O_3 ratios (in A); Th/Al_2O_3 vs. Sc/Al_2O_3 ratios (in B)

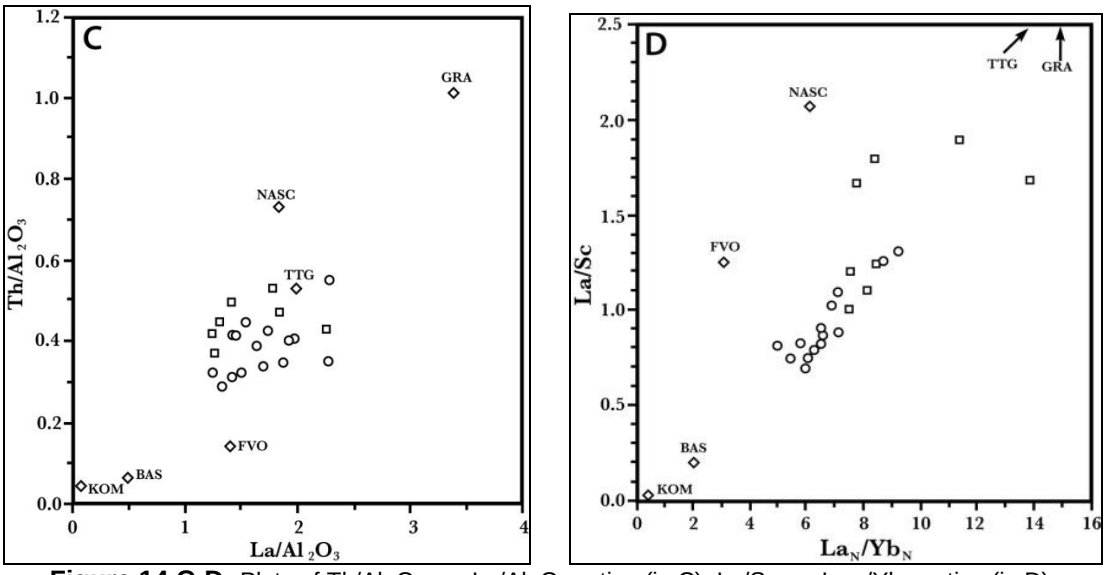

Figure 14 C-D: Plots of Th/Al_2O_3 vs. La/Al_2O_3 ratios (in C), La/Sc vs. La_N/Yb_N ratios (in D).

5.3. Pb-, Sr- and Nd-isotopic behavior and implication for crustal development

The Sm-Nd, Rb-Sr and Pb-Pb isotopic systematics were analyzed in the FTG and MG shales. The Pb isotopic compositions were measured in ten FTG samples with the data fitting a linear array that corresponds to a Pb-Pb age of 2596±12 Ma (MSWD = 12.8; Fig. 15), while the Pb-isotope composition of seven MG rocks is less constrained (MSWD = 176) with a line providing an age of 2231±31 Ma. All FTG and MG samples were also analyzed by the Sm-Nd and Rb-Sr methods. The data points of the FTG shales, when plotted in a Rb-Sr isochron diagram, plot along an array corresponding to an age of 2735±32 Ma with an initial $^{87}Sr/^{86}Sr$ = 0.7143±0.0017 and an MSWD = 41.8 (Fig. 16). The two anomalous samples (79NC116 and 79NC117) plot away from the best-fit line. By excluding these two data from isochron calculation, the linear array improves substantially with an MSWD = 2.18, and an age at 2939±38 Ma with an initial $^{87}Sr/^{86}Sr$ = 0.7074±0.0020. The Rb-Sr isotope data for the MG shales display a considerable scatter (MSWD = 211); the best fit line corresponding to an age of 2321±50 Ma and an initial $^{87}Sr/^{86}Sr$ = 0.7219±0.0023.

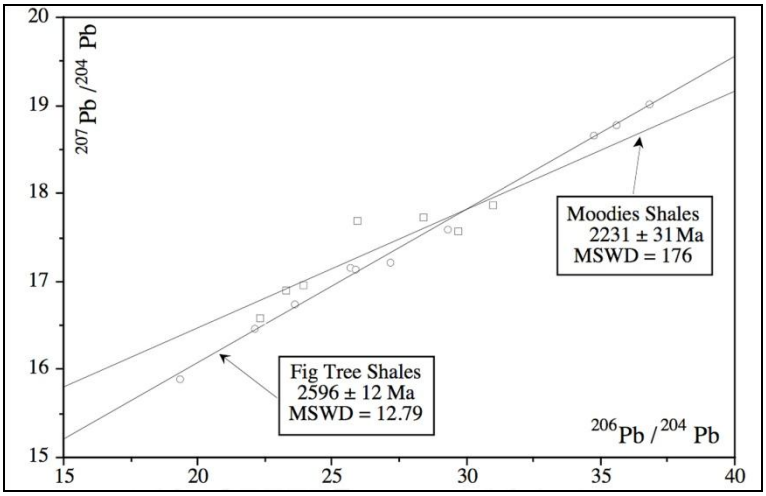

Figure 15: Pb-Pb isochron diagram for the FTG (circles) and MG (squares) shales.

The Sm-Nd isotope data scatter so much that they have not been considered for age calculation. All three isotopic systems indicate ages, if any, which are much younger than the

expected depositional age of the sediments. This suggests in turn that alteration caused by either a thermal or a chemical event, reset and/or disturbed the isotopic systems, most probably at ~2.6 to 2.7 Ga, as a result of large-scale fluid migrations. This process of resetting is not unusual (Perry and Turekian, 1974) and has also been reported and discussed in detail in other rocks of the BGB, such as komatiites (Gruau et al., 1990; Lécuyer et al., 1994; Lahaye et al., 1995), felsic volcanics (Allsopp et al., 1973) and, more recently, metagreywackes (Toulkeridis et al., 1999), barites (De Ronde et al., 1991) and carbonates (Toulkeridis et al., 1998) of the FTG.

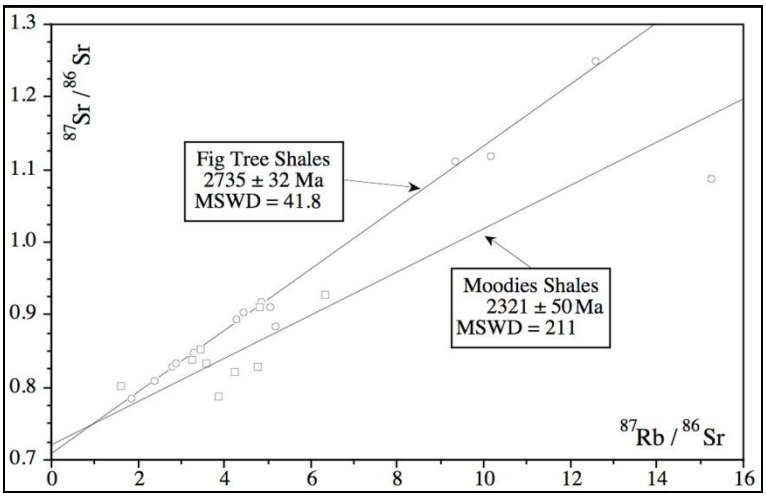

Figure 16: Rb-Sr isochron diagram for the FTG (circles) and MG (squares) shales.

The FTG and MG shales average a $^{147}Sm/^{144}Nd$ ratio of about 0.123 and 0.110, respectively, and therefore yield a normal upper crustal ratio (~0.12; McCulloch and Wasserburg, 1978). The MG sample 79NC127 has a ratio identical to those of the FTG samples, while the FTG sample 79NC107 has a ratio that matches the range of the MG shales (Fig. 17). The FTG shales have also a higher average $^{143}Nd/^{144}Nd$ ratio than the MG shales. The same ratios of the FTG shales are also consistent with those from previously published studies (McCulloch and Wasserburg, 1978; Miller and O'Nions, 1985; Dia et al., 1990) and, more generally, with those of Archaean shales (McLennan and Hemming, 1992). The decrease in the Sm/Nd isotope ratio from FTG to MG shales most probably reflects a change in the source of the shales from relatively undifferentiated mafic upper-crustal compositions to more differentiated felsic compositions.

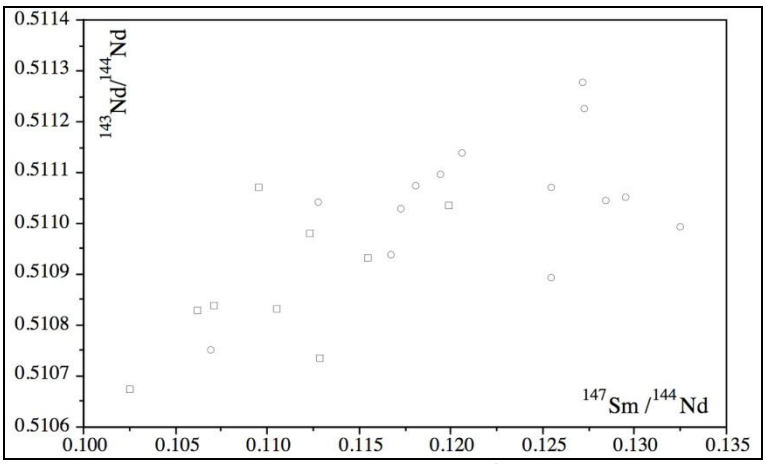

Figure 17: Diagram of $^{147}Sm/^{144}Nd$ vs. $^{143}Nd/^{144}Nd$ ratios of the FTG (circles) and MG (squares) shales.

Depleted-mantle model ages (TDM) were calculated by using an average crustal ratio of 0.11 and the Nd model age parameters of Goldstein et al. (1984; Table 5). The T_{DM} ages for shales have been tested often as useful tools for the reconstruct of either the origin and/or the provenance of these rocks (e.g., Allègre and Rousseau, 1984; André et al., 1986). Here, the T_{DM} ages range between ~3.2 and 3.9 Ga for the FTG shales, and between 3.0 and 3.6 Ga for the MG shales. The fact that some T_{DM} ages are younger than the depositional ages can be explained by heterogeneous mantle sources (Gruau et al., 1990). The T_{DM} ages of ~3.3 to 3.6 Ga are within the age range of the underlying rocks from Onverwacht Group, making them potential sources of the FTG and MG shales (Fig. 18). Older T_{DM} ages may be too high, but they can be explained by the presence of early phases of granitoïd rocks surrounding the BGB, such as the gneisses of the Ancient Gneiss Complex, and granitoïd rocks (tonalites-trondjhemites-granodiorites and granites) juxtaposed south of the BGB (Fig. 18), of which zircon ages as high as 3.7 Ga were obtained (Compston and Kröner, 1988; Kröner et al., 1996). Although sedimentary sorting possibly affects the TDM ages of sedimentary rocks (McLennan et al., 1989), the shales of the BGB appear to have remained fairly undisturbed in this respect.

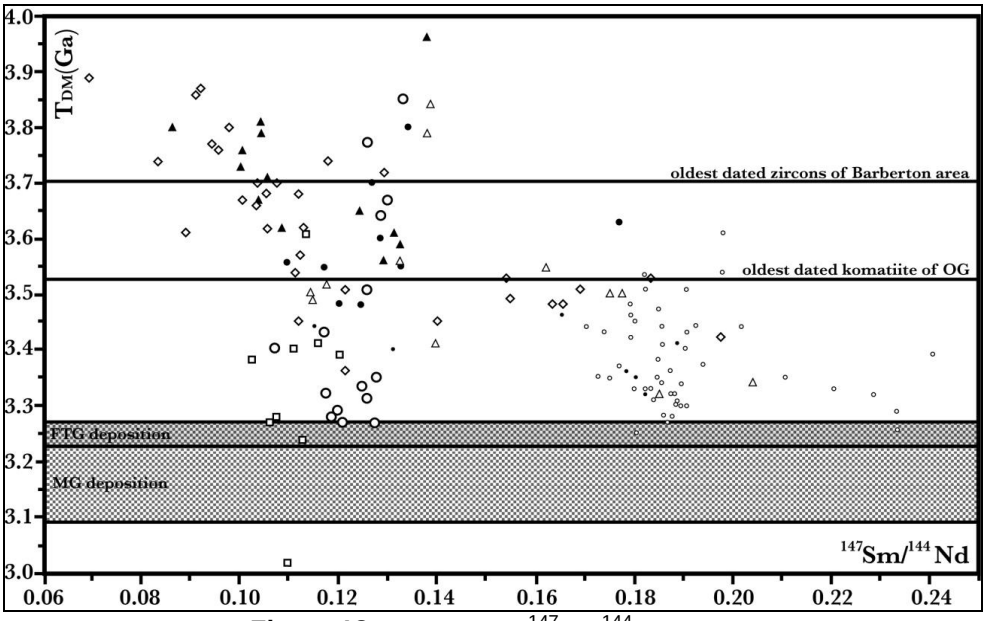

Figure 18: T_{DM} (Ga) vs. $^{147}Sm/^{144}Nd$ ratios.

Calculated ε_{Nd} values for t = 3245 and 3200 Ma vary between -5.35 and +3.96 for the FTG shales, and between -3.14 and +4.84 for the MG shales, implying mixed mafic-felsic mantle-crustal sources in different proportions. The value of approximately +5 is obviously too high, since even mantle samples at ~3.2 Ga did not have such high values (Fig. 19; Hamilton et al., 1979; Jahn et al., 1982; Lecuyer et al., 1994). The simplest explanation is that the Sm-Nd system was opened since the time of deposition of the sediments as a result of a REE fractionation at distinct periods (Bock et al., 1994). In figure 20, different intersections of the FGT samples can be seen, as a function of time, in the evolution lines of ε_{Nd}, with a model of the depleted mantle.

The large variations of the ε_{Nd} ratio may also be explained by the impact of a carbonatization (Gruau et al., 1990; 1992; Tourpin et al., 1991). The variability of initial ε_{Nd} -values in the shales can possibly be attributed to an isotopic exchange of Nd with surrounding rocks during alteration, and a further fractionation of the Sm/Nd ratio during later events (Lahaye et al., 1995), as already suggested by the Rb-Sr and Pb-Pb isotopic data (Figs. 15, 16 and 20). Therefore, recalculation of the ε_{Nd} values with initial "alteration ages" of about 2.6 to 2.7 Ga provides lower and consequently more meaningful ε_{Nd} -values.

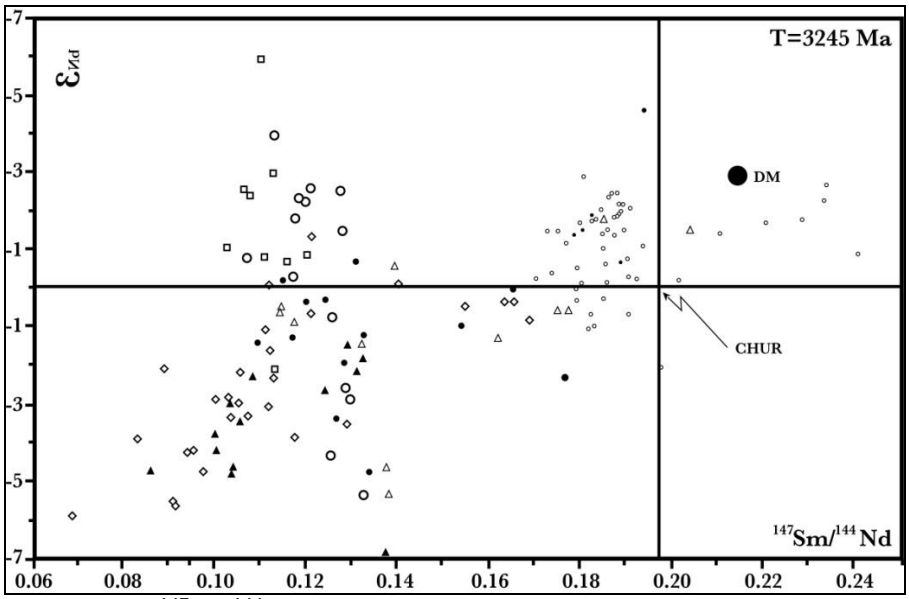

Figure 19: ε_{Nd} vs. $^{147}Sm/^{144}Nd$ ratios at T = 3245 Ma of the FTG and MG shales, together with previously published isotopic values of FTG shales compared to possible source rocks.

It has often been reported that Sm-Nd isotopic data from rock suites of early Archaean provinces that were subjected to metamorphic and/or metasomatic events long after deposition or crystallization, reflect open-system behaviors that lead to noticeable resetting of the Sm-Nd system, which is accompanied by Nd-isotopic homogenization (Toulkeridis et al., 1998). Therefore, caution should be used in interpreting highly variable, apparent initial ε_{Nd} values of ancient rocks in terms of long-lasting regional mantle heterogeneity, such as for the shales studied here, which ε_{Nd} values scatter widely over a range of 9 units.

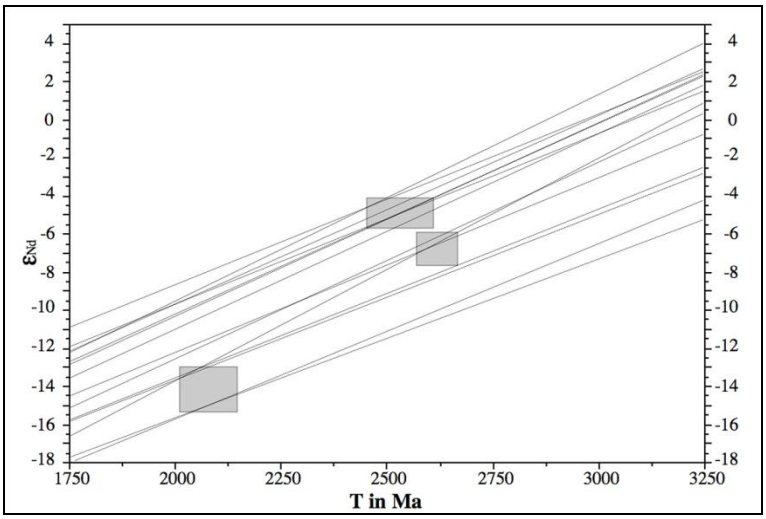

Figure 20: ε_{Nd} vs. time plot for Nd isotope data of the FTG shales.

5.4. Is there a missing link in the estimated source?

The provenance of all studied shales has been discussed, and the rocks appear to be of mixed origin including a mafic-to-ultramafic and a felsic source. The Nd isotope data suggest an additional possible input. Plotting all data of plutonic, volcanic and sedimentary rocks of the BGB and of the surrounding area in a same diagram confirms that one source is missing.

Available data of the komatiites and basalts yield slightly positive and slightly negative ε_{Nd} values at time t = 3245 Ma, with $^{147}Sm/^{144}Nd$ ratios of 0.17 and higher, while the granititoïd rocks of the same area at the same period, and the gneisses of the Ancient Gneiss Complex have negative ε_{Nd} values with $^{147}Sm/^{144}Nd$ ratios of 0.14 and lower. The clastic sedimentary rocks of the BGB studied here and the greywackes of previous studies (Dia et al., 1990; Toulkeridis et al., 1999) have negative and positive ε_{Nd} values, but the positive values are higher than any yet reported possible source rock. It might, therefore, be speculated that the felsic volcanics of the interior FTG, which are intercalated within the sedimentary sequence, may represent the missing link to the source displayed by the Nd isotopic values. These felsic volcanics could have highly variable ε_{Nd} values as a result of their plutonic source below the BGB. They could, therefore, reflect mixing with mafic volcanics while intruding these rocks before deposition of the Barberton sediments.

6. CONCLUSIONS

Mineralogical data combined with geochemical parameters are useful indicators for the search of the provenance of ancient shales. However, chemical compositions have to be interpreted and used carefully if the possibility exists of the occurrence of secondary effects, such as weathering, thermal alteration or hydraulic sorting. For instance, Rb-Sr, Pb-Pb and Sm-Nd results may be misinterpreted as depositional ages, as they can reflect open-system behaviors severely disturbed and rehomogenized during later thermal and/or chemical events.

Mineral, chemical and Rb-Sr, Sm-Nd and Pb-Pb isotopic data were determined on shales of the ~3.5-3.1 Ga old Barberton Greenstone Belt in South Africa. A progressive chemical change in the composition can be followed upwards the sedimentary sequence from an ultramafic-mafic to a felsic-plutonic source. The SiO_2, K_2O, U, Rb, Ba, Sr contents systematically increase as well as the Zr/Y ratio, and the MgO and Fe_2O_3 contents systematically decrease as well as the Sm/Nd and Cr/Zr ratios. Both sets of rocks yield high concentrations of Cr and Ni relative to other Archaean shales.

The shales of the Fig Tree Group have varied REE patterns with lower La_N/Yb_N ratios of 6.6±1.9 and Eu/Eu* ratios of 0.86±0.11, than those of the Moodies Group with La_N/Yb_N ratios of 8.8±4.6 and Eu/Eu* ratios of 0.91±0.18. An increase in the Gd_N/Yb_N, Th/Sc, La/Sc, La/Yb ratios, and a decrease in the Sm/Nd ratio appear to reflect a change from a relatively undifferentiated mafic upper-crustal source to a more differentiated felsic composition.

The T_{DM} Sm-Nd ages also suggest partly differentiated mantle sources. However, they do so predominantly with either the mafic rocks of the lower Greenstone Belt itself, or the surrounding granitoid rocks as the potential source(s) of the shales. The Rb-Sr and Pb-Pb isotopic ages provide strong evidence for an alteration process caused by either a thermal or a chemical event that, at least, disturbed the isotopic systems of the studied samples, as a result of large-scale fluid migrations.

ACKNOWLEDGMENTS

We would like to expresses our sincere thanks to P. Karcher, J. Samuel, B. Kiefel and D. Tisserant (CGS-CNRS/ULP, Strasbourg), E. Mackiolzyk (Max-Planck-Institut, Mainz) and N. Groshopf (University of Mainz) for technical assistance during the course of the study. Financial support by the Deutsche Forschungsgemeinschaft (DFG) (Grant Kr-590/34) and the German-French exchange program "Programme de Coopération Scientifique" is also gratefully acknowledged.

REFERENCES

1. Aira, M., F. Monroy, and J. Dominguez. 2006. Eisenia foetida (Oligochaeta, Lumbricidae) activates fungal growth, triggering cellulose decomposition during vermicomposting. Microbial Ecology 52 (4):738-747.
2. Allègre, C.J. and Rousseau, D., 1984. The growth of the continent through geological time studies by Nd isotope analysis of shales. Earth Planet. Sci. Lett. 67, 19-34.
3. Allsopp, H.L., Viljoen, M.J. and Viljoen, R.P., 1973. Strontium isotopic studies of the mafic and felsic rocks of the Onverwacht Group of the Swaziland Sequence. Geol. Rundsch. 62, 902-917.
4. Anhaeusser, C.R. and Robb, L.J., 1981. Magmatic cycles and the evolution of the Archean granitic crust in the eastern Transvaal and Swaziland. Spec. Publ. Geol. Soc. Aust. 7, 457-467.
5. Anhaeusser, C.R., 1973. The evolution of the early Precambrian crust of southern Africa. Phil. Trans. Roy. Soc. Lond. A., 273, 359-388.
6. Anhaeusser, C.R., Robb, L.J. and Viljoen, M.J., 1983, Notes on the provisional geological map of the Barberton Greenstone Belt and surrounding granitic terrane, eastern Transvaal and Swaziland (1:250000 colour map). Spec. Publ. Geol. Soc. S. Afr. 9, 221-223.
7. Armstrong, R.A., Compston, W., DeWit, M.J. and Williams, I.S., 1990. The stratigraphy of the 3.5-3.2 Ga Barberton Greenstone Belt revisited: a single zircon ion microprobe study. Earth Planet. Sci. Lett. 101, 90-106.
8. Balistieri, L.S. and Murray, J.M., 1984. Marine scavenging: trace metal adsorption by interfacial sediment from MANOP Site H. Geochim. Cosmochim. Acta 48, 921-929.
9. Barton, J.M.Jr., Robb, I.J., Anhaeusser, C.R. and Van Nierop, D.A., 1983. Geochronologic and Sr-isotopic studies of certain units in the Barberton granit-greenstone terrane, South Africa. Spec. Publ. Geol. Soc. S. Afr. 9, 63-72.
10. Bierlein, F.P., 1995. Rare-earth element geochemistry of clastic and chemical metasedimentary rocks associeted with hydrothermal sulphide mineralisation in the Olary Block, South Australia. Chem. Geol. 122, 77-98.
11. Bock, B., McLennan, S.M. and Hanson, G.N., 1994. Rare earth element redistribution and its effects on the Neodymium isotope system in the Austin Glen Member of the Normanskill Formation, New York, USA. Geochim. Cosmochim. Acta 58, 5245-5253.
12. Bonjour, J.L. and Dabard, M.P., 1991. Ti/Nb ratios of clastic terrigenous sediments used as an indicator of provenance. Chem. Geol. 91, 257-267.
13. Cameron, A.E., Smith, D.H. and Walker, R.L., 1969. Mass spectrometry of nanogram-size samples of lead. Anal. Chem. 41, 525-526.
14. Chaudhuri, S., Stille, P. and Clauer, N., 1992. Sm-Nd isotopes in fine-grained clastic sedimentary materials: clues to sedimentary processes and recycling growth of the continental crust. In: Clauer, N. and Chaudhuri, S. (Eds) Isotopic signatures and sedimentary records. Lecture Notes in Earth Sciences 43. Springer, Berlin, Heidelberg, New York. 287-319.
15. Cloete, M., 1991. An overview of metamorphism in the Barberton Greenstone Belt. In: L.D. Ashwal (ed.), Two Cratons and an Orogen - Excursion guidebook and review articles for a field workshop through selected Archaean terranes of Swaziland, South Africa and Zimbabwe. IGCP Project 280, Dept. of Geology, Univ. Witwatersrand, Johannesburg. 84-98.
16. Compston, W. and Kröner, A., 1988. Multiple zircon growth within early Archaean tonalitic gneisses from the Ancient Gneiss Complex, Swaziland. Earth Planet. Sci. Lett. 87, 13-28.
17. Condie, K.C. and Wronkiewicz, D.J., 1990. The Cr/Th ratio in Precambrian pelites from the Kaapvaal Craton as an index of craton evolution. Earth Planet. Sci. Lett. 97, 256-267.
18. Condie, K.C., 1967. Geochemistry of early Precambrian greywackes from Wyoming. Geochim. Cosmochim. Acta 31, 2135-2149.

19. Condie, K.C., 1991. Another look at rare earth elements in shales. Geochim. Cosmochim. Acta 55, 2527-2531.
20. Condie, K.C., 1993. Chemical composition and evolution of the upper continental crust: Contrasting results from surface samples and shales. Chem. Geol. 104, 1-37.
21. Condie, K.C. and Martell, C., 1983. Early Proterozoic metasediments from north-central Colorado: Metamorphism, provenance, and tectonic setting. Geol. Soc. Amer. Bull. 94, 1215-1224.
22. Crighton, J.G. and Condie, K.C., 1993. Trace elements as source indicators in cratonic sediments: a case study from the Early Proterozoic Libby Creek Group, southeatern Wyoming. Journ. Geol. 101, 319-332.
23. Cullers, R.L., Yeh, L. and Chaudhuri, S., 1974. Rare earth elements in Silurian pelitic schists from NW Maine. Geochim. Cosmochim. Acta 38, 389-400.
24. Cullers, R.L., Chaudhuri, S, Kilbane, N. and Koch, R., 1979. Rare-earths in size fractions and sedimentary rocks of Pennsylvanian-Permian age from the mid-continent of the USA. Geochim. Cosmochim. Acta 43, 1285-1301.
25. Danchin, R.V., 1967. Chromium and nickel in the Fig Tree Shale from South Africa. Science 158, 261-262.
26. Deer, W.A., Howie, R.A. and Zussman, J., 1983. An introduction to the rock forming minerals. J.Wiley and Sons, New York 528pp.
27. De Ronde, C.E.J., Hall, C.M., York, D. and Spooner, E.T.C., 1991. Laser step-heating 40Ar/39Ar age spectra from early Archean (~3.5 Ga) Barberton greenstone belt sediments: A technique for detecting cryptic tectono-thermal events. Geochim. Cosmochim. Acta 55, 1933-1951.
28. DeWit, M.J., Hart, R., Martin, A. and Abbott, P., 1982. Archean abiogenic and probable bio-genic structures associated with mineralized hydrothermal vent systems and regional metasomatism, with implications for Greenstone Belt studies. Econ. Geol. 77, 1783-1802.
29. Dia, A., Allègre, J. and Erlank, A.E., 1990. The development of continental crust through geological time: the South African case. Earth Planet. Sci. Lett. 98, 74-89.
30. Eriksson, K.A., Krapez, B. and Fralick, P.W., 1994. Sedimentology of Archean greenstone belts: signatures of tectonic evolution. Earth Sci. Rev. 37, 1-88.
31. Eriksson, K.A., Taylor, S.R. and Korsch, R.J., 1992. Geochemistry of 1.8-1.67 Ga mudstones and siltstones from the Mount Isa Inlier, Queensland, Australia: Provenance and tectonic implications. Geochim. Cosmochim. Acta 56, 899-909.
32. Eriksson, P.G., Twist, D., Snyman, C.P. and Burger, L., 1990. The geochemistry of the Silverton Shale Formation, Transvaal Sequence. South Afr. Journ. Geol. 93, 454-462.
33. Fedo, C.M., Eriksson, K.A., Krogstad, E.J., 1996. Geochemistry of shales from the Archaean (3.0 Ga) Buhwa Greenstone Belt, Zimbabwe: implications for provenance and source-area weathering. Geochim. Cosmochim. Acta 60, 1751-1763.
34. Folk, R.L., 1974. Petrology of sedimentary rocks: Austin, TX, Hemphill's 170pp.
35. Gao , S. and Wedepohl, K.H., 1995. The negative Eu anomaly in Archean sedimentary rocks: Implications for decomposition, age and importance of their granitic sources. Earth Planet. Sci. Lett. 133, 81-94.
36. Garver, J.I., Royce, P.R. and Smick, T.A., 1996. Chromium and nickel in shale of the Taconic foreland: a case study for the provenance of fine-grained sediments with an ultramafic source. J. Sediment. Res. 66. 100-106.
37. Goldstein, S.L., O`Nions, R.K. and Hamilton, P.J., 1984. A Sm-Nd isotopic study of atmospheric dusts and particulates from major river systems. Earth Planet. Sci. Lett. 70, 221-236.
38. Gromet, L.P., Dymek, R.F., Haskin, L.A. and Korotev, R.L., 1984. The North American Shale Composite: its compilation, major and trace element characteristics. Geochim. Cosmochim. Acta 48, 2469-2482.
39. Gruau, G., Chauvel, C. and Jahn, B.M., 1990. Anomalous Sm-Nd ages for the early Archean Onverwacht Group volcanics. Contrib. Mineral. Petrol. 104, 27-34.
40. Gruau, G., Tourpin, S., Fourcade, S. and Blais, S., 1992. Loss of isotopic (Nd, O) and chemical (REE) memory during metamorphism of komatiites: new evidence from eastern Finland. Contrib. Mineral. Petrol. 112, 66-82.

41. Hamilton, P.J., Evensen, N.M., O´Nions, R.K., Smith, H.S. and Erlank, A.J., 1979. Sm-Nd dating of Onverwacht Group volcanics, southern Africa. Nature 279, 298-300.
42. Harnois, L., 1988. The CIW index: a new chemical index of weathering. Sedim. Geol. 55, 319-322.
43. Hayashi, T., Tanimizu, M., Tanaka, T., 2004. Origin of negative Ce anomalies in Berberton sedimentary rocks, deduced from La-Ce and Sm-Nd isotope systematics. Prec. Res. 135, 345-357.
44. Hemming, S.R., McLennan, S.M. and Hanson, G.N., 1995. Geochemical and Nd/Pb isotopic evidence for the provenance of the Early Proterozoic Virginia Formation, Minnesota. Implications for the tectonic setting of the Animikie basin. Journ. Geol. 103, 147-168.
45. Heubeck, C., Wendt, J.I., Toulkeridis, T., Kröner, A. and Lowe, D.R., 1993. Timing of Deformation of the Archaean Barberton Greenstone Belt, South Africa: Constraints from Zircon dating of the Salisbury Kop Pluton. Journ. Geol. Soc. S. Afr. 93, 1-8.
46. Heubeck, C. and Lowe, D.R., 1994a. Late syndepositional deformation and detachment tectonics in the Barberton Greenstone Belt, South Africa. Tectonics 13, 1514-1536.
47. Heubeck, C. and Lowe, D.R., 1994b. Depositional and tectonic setting of the Archean Moodies Group, Barberton Greenstone Belt, South Africa. Prec. Res. 68, 257-290.
48. Hofmann, A., 2005. The geochemistry of sedimentary rocks from the Fig Tree Group, Barberton greenstone belt: Implications for tectonic, hydrothermal and surface processes during mid-Archean times. Prec. Res. 143, 23-49.
49. Hofmann, A., Bolhar, R., Dirks, P.H.G.M., Jelsma, H.A., 2003. The geochemistry of Archean shales derived from a mafic volcanic sequence, Belingwe greenstone belt, Zimbabwe: provenance, source area unroofing and submarine vs. subaerial weathering. Geochim. Cosmochim. Acta 67, 421-440.
50. Honty, M., Clauer N., and Šucha V., 2008. Rare-earth element systematics of mixed-layered illite-smectite from sedimentary and hydrothermal environments of the Western Carpathians (Slovakia). Chem. Geol. 249, 167-190.
51. Jahn, B.M., Gruau, G. and Glikson, A.Y., 1982. Komatiites of the Onverwacht Group, S. africa: REE geochemistry, Sm/Nd age and mantle evolution. Contrib. Mineral. Petrol. 80, 25-40.
52. Jahn, B.M, and Condie, K.C., 1995. Evolution of the Kaapvaal Craton as viewed from geochemichal and Sm-Nd isotopic analyses of intracratonic pelites. Geochim. Cosmochim. Acta 59, 2239-2258.
53. Jenner, G.A., Fryer, B.J. and McLennan, S.M., 1981. Geochemistry of the Archean Yellowknife Supergroup. Geochim. Cosmochim. Acta 45, 1111-1129.
54. Kamo, S.L. and Davis, 1993. Reassessment of Archean crustal development in the Barberton Mountain Land, South Africa, based on U-Pb dating. Tectonics 13, 167-192.
55. Krogh, T.E., 1973. A low-contamination method for hydrothermal decomposition of zircon and extraction of U and Pb for isotopic age determinations. Geochim. Cosmochim. Acta 9, 1-32.
56. Kröner, A. and Todt, W., 1988. Single zircon dating constraining the maximum age of the Barberton greenstone belt, southern Africa. Journ. Geophys. Res. 93, 15329-15337.
57. Kröner, A., Compston, W. and Williams, I.S., 1989. Growth of early Archaean crust in the Ancient Gneiss Complex of Swaziland as revealed by single zircon dating. Tectonophysics 161, 271-298.
58. Kröner, A., Byerly, G.R. and Lowe, D.R., 1991. Chronology of early Archean granite-greenstone evolution in the Barberton Mountain Land, South Africa, based on precise dating by single zircon evaporation. Earth Planet. Sci. Lett. 103, 41-54.
59. Kröner, a., Wendt, J.I., Milisenda, C., Compston, W. and Maphalala, R., 1993. Zircon geochronology and Nd isotopic systematics of the Ancient Gneiss Complex, Swaziland, and implications for crustal evolution. Geol. Surv. Mines Dept., Swaziland, Bull 11, 15-37.
60. Kröner, A., Hegner, E., Wendt, J.I., Byerly, G.R. and Todt, W., 1996. The oldest part of the Barberton granitoid-greenstone terrain, South Africa: evidence for crust formation between 3.5 and 3.7 Ga. Prec. Res. 78, 105-124.

61. Lahaye, Y., Arndt, N., Byerly, G., Chauvel, C., Fourcade, S. and Gruau, G., 1995. The influence on the trace element and Nd isotopic compositions of komatiites. Chem. Geol. 126, 43-64.
62. Lécuyer, C., Gruau, G., Anhaeusser, C.R. and Fourcade, S., 1994. The origin of fluids and the effects of metamorphism on the primary chemical compositions of Barberton komatiitets: New evidence from geochemical (REE) and isotopic (Nd, O, H, 39Ar/40Ar) data. Geochim. Cosmochim. Acta 58, 969-984.
63. Lopez-Martinez, M.D., York, D. and Hanes, J.A., 1992. A 40Ar/39Ar geochronological study of komatiites and komatiitic basalts from the lower Onverwacht volcanics: Barberton Mountain Land, South Africa. Prec. Res. 57, 91-119.
64. Lowe, D.R. and Byerly, G.R., 1999. Stratigraphy of the west-central part of the Barberton Greenstone Belt, South Africa. In: Lowe, D.R. and Byerly, G.R. (Eds.), Geologic Evolution of the Barberton Greenstone Belt, South Africa: Geol. Soc. Amer. Spec. Pap. 329, 1-36.
65. Lowe, D.R. and Nocita, B.W., 1999. Foreland basin sedimentation in the Mapepe Formation, southern-facies Fig Tree Group: In: Lowe, D.R. and Byerly, G.R. (Eds.), Geologic Evolution of the Barberton Greenstone Belt, South Africa: Geol. Soc. Amer. Spec. Pap. 329, 233-258.
66. Lowe, D.R., 1991. Geology of the Barberton Greenstone Belt: an overview. In: L.D. Ashwal (Ed.), Two Cratons and an Orogen - Excursion guidebook and review articles for a field workshop through selected Archean terranes of Swaziland, South Africa and Zimbabwe. IGCP Project 280, Dept. of Geology, Univ. Witwatersrand, Johannesburg 47-58.
67. Manceau, A. and Calas, G., 1986. Nickel-bearing clay minerals: II. Intracrystalline distribution of nickel: An X-ray adsorption study. Clay Min. 21, 341-360.
68. Maas, R. and McCulloch, M.T., 1991. The provenance of Archean clastic metasediments in the Narryer Gneiss Complex, Western Australia: trace element geochemistry, Nd isotopes, and U-Pb ages for detrital zircons. Geochim. Cosmochim. Acta 55, 1915-1932.
69. McCulloch, M.T. and Wasserburg, G.J., 1978. Sm-Nd and Rb-Sr chronology of continental crust formation. Science 200, 1003-1011.
70. McDaniel, D.K., Hemming, S.R., McLennan, S.M. and Hanson, G.N., 1994. Petrographic, geochemical, and isotopic constraints on the provenance of the early Proterozoic Chelmsford Formation, Sudbury basin, Ontario. Journ. Sedim. Res. A64, 362-372.
71. McLennan, S.M. and Hemming, S., 1992. Samarium/neodymium elemental and isotopic systematics in sedimentary rocks. Geochim. Cosmochim. Acta 56, 887-898.
72. McLennan, S.M. and Taylor, S.R., 1991. Sedimentary rocks and crustal evolution: Tectonic setting and secular trends. Journ. Geol. 99, 1-21.
73. McLennan, S.M., 1982. On the geochemical evolution of sedimentary rocks. Chem. Geol. 37, 335-350.
74. McLennan, S.M., 1989. Rare earth elements in sedimentary rocks: influence of provenance and sedimentary processes. Rev. Mineral. 21, 169-200.
75. McLennan, S.M., Nance, W.B. and Taylor, S.R., 1980. Rare earth element-thorium correlations in sedimentary rocks, and the composition of the continental crust. Geochim. Cosmochim. Acta 44, 1833-1839.
76. McLennan, S.M., Taylor, S.R. and Eriksson, K.A., 1983a. Geochemistry of Archean shales from the Pilbara Supergroup, Western Australia. Geochim. Cosmochim. Acta 47, 1211-1222.
77. McLennan, S.M., Taylor, S.R. and Kröner, A., 1983b. Geochemical evolution of Archean shales from South Africa. I. The Swaziland and Pongola Supergroups. Prec. Res. 22, 93-124.
78. McLennan, S.M., Taylor, S.R. and McGregor, V.R., 1984. Geochemistry of Archean metasedimentary rocks from West Greenland. Geochim. Cosmochim. Acta 48, 1-13.
79. McLennan, S.M., McCulloch, M.T., Taylor, S.R. and Maynard, J.B., 1989. Effects of sedimentary sorting on neodymium isotopes in deep-sea turbidites. Nature 337, 547-549.

80. McLennan, S.M., Hemming, S., McDaniel, D.K. and Hanson, G.N., 1993. Geochemical approaches to sedimentation, provenance, and tectonics. Geol. Soc. Amer., Spec. Pap. 284, 21-40.
81. Miller, R.G. and O'Nions, R.K., 1985. Source of Precambrian chemical and clastic sediments. Nature 314, 325-330.
82. Morad, S. and Aldahan, A.A., 1985. Leucoxene-calcite-quartz aggregates in sandstones and the relation to decomposition of sphene. N. Jb. Miner., Mh. 1985, 458-468.
83. Morad, S. and Aldahan, A.A., 1985. Authigenic sphene in sandstones of the Brøttum Formation (Norway) and the Dala Sandstone (Sweden). N. Jb. Miner., Mh. 1986, 135-144.
84. Nance, W.B. and Taylor, S.R., 1977. Rare earth element patterns and crustal evolution - II. Archean sedimentary rocks from Kalgoorlie, Australia. Geochim. Cosmochim. Acta 41, 225-231.
85. Nesbitt, H.W. and Young, G.M., 1982. Early Proterozoic climates and plate motions inferred from major alement chemistry of lutites. Nature 299, 715-717.
86. Nesbitt, H.W. and Young, G.M., 1984. Prediction of some weathering trends of plutonic and volcani rocks based on thermodynamic and kinetic considerations. Geochim. Cosmochim. Acta 48, 1523-1534.
87. Nesbitt, H.W. and Young, G.M., 1989. Formation and diagenesis of weathering profiles. Journ. Geol. 97, 129-147.
88. Nesbitt, H.W., Markovics, G. and Price, R.C., 1980. Chemical processes affecting alkalies and alkaline earths during continental weathering. Geochim. Cosmochim. Acta 44, 1659-1666.
89. Nocita, B.W. and Lowe, D.R., 1990. Fan-delta sequence in the Archean Fig Tree Group, Barberton Greenstone Belt, South Africa. Prec. Res. 48, 375-393.
90. Panhuys-Sigler, van M. and Trewin, N.H., 1990. Authigenic sphene cement in Permian sandstones from Arran. Scott. Journ. Geol. 26, 139-144.
91. Perry, K.A. and Turekian, K.K., 1974. The effect of diagenesis on the redistribution of strontium isotopes in shales. Geochim. Cosmochim. Acta 38, 929-935.
92. Reimer, T.O., 1980. Archean sedimentary baryte deposits of the Swaziland Supergroup (Barberton Mountain Land, South Africa). Prec. Res. 12, 393-410.
93. Reimer, T.O., 1985: Rare earth elements and the suitability of shales as indicators for the composition of the Archaean continental crust. N. Jb.. Miner., Abh., 152: 211-223.
94. Roaldset, E., 1973. Rare earth elements in Quaternary clays of the Numedal area, southern Norway. Lithos 6, 349-372.
95. SACS (South African Committee for Stratigraphy), 1980. Stratigraphy of South Africa: Part I: Lithostratigraphy of the Republic of South Africa, South West Africa/Namibia and the Republics of Bophuthatswana, Transkai, and Venda. Geol. Surv. of S. Africa, Handbook 8, 690pp.
96. Samuel, J., Rouault R., and Besnus Y., 1985. Analyse multi-élémentaire standardisée des matériaux géologiques en spectrométrie d'émission par plasma à couplage inductif. Analusis 13, 312-317.
97. Schaltegger, U., Stille, P., Rais, N., Piqué, A., and Clauer, N., 1994. Nd and Sr isotopic dating of diagenesis and low-grade metamorphism of argillaceous sediments: Geochim. Cosmochim. Acta 58,1471-1481.
98. Schieber, J., 1988. Redistribution of rare-earth elements during diagenesis of carbonate rocks from the Mid-Proterozoic Newland Formation, Montana, USA. Chem. Geol. 69, 111-126.
99. Stern, W.B., 1972. Zur röntgenspektrometrischen Analyse von silikatischen Gesteinen und Mineralien. Schweiz. Mineral. Petrogr. Mitt. 52, 1-25.
100. Taylor, S.R. and McLennan, S.M., 1985. The continental crust: its composition and evolution. Oxford, Blackwell 312 pp.
101. Taylor, S.R., Rudnick, R.L., McLennan, S.M. and Eriksson, K.A., 1986. Rare earth element patterns in Archean high grade metasediments and their tectonic significance. Geochim. Cosmochim. Acta 50, 2267-2279.

102. Toulkeridis, T., Goldstein, S.L., Clauer, N., Kröner, A. Lowe, D.R., 1994. Sm-Nd dating of Fig Tree Clays: implications for the thermal history of the Barberton Greenstone Belt, South Africa. Geology 22, 199-202.
103. Toulkeridis, T., Clauer, N. and Kröner, A., 1996. Origin of the chemical variations of clay minerals in early Archean sediments, Barberton Greenstone Belt (South Africa). Prec. Res. 79, 195-207.
104. Toulkeridis, T., Goldstein, S.L., Clauer, N., Kröner, A., Todt, W. and Schidlowski, M., 1998. Sm-Nd, Rb-Sr, Pb-Pb dating of carbonates from the early Archaean Barberton Greenstone Belt, South Africa: evidence for post-depositional isotopic resetting at low temperature. Prec. Res. 92, 129-144.
105. Toulkeridis, T., Clauer, N., Goldstein, S.L., Kröner, A., Reimer, T. and Todt, W., 1999. Characterization, provenance, and tectonic setting of Fig Tree greywackes from the Archaean Barberton Greenstone Belt, South Africa. J. Sed. Geol. 124, 113-129.
106. Tourpin, S., Gruau, G., Blais, S. and Fourcade, S., 1991. Resetting of REE, and Nd and Sr isotopes during carbonitization of a komatiite flow from Finland. Chem. Geol. 90, 15-29.
107. Veizer, J. and Garret, D.E., 1978. Secular variations in the composition of sedimentary carbonate rocks, I. Alkali metals. Prec. Res. 6, 367-380.
108. Veizer, J., 1978. Secular variations in the composition of sedimentary carbonate rocks. II. Fe, Mn, Ca, Mg, Si and minor constituents. Prec. Res. 6, 381-413.
109. Viljoen, M.J. and Viljoen, R.P., 1969. An introduction to the geology of the Barberton granite-greenstone terrain. Geol. Soc. S. Africa, Spec. Publ. 2, 9-28.
110. Weis, D., and Wasserburg, G.J., 1987. Rb-Sr and Sm-Nd isotope geochemistry and chronology of cherts from the Onverwacht Group (3.5 AE), South Africa: Geochim. Cosmochim. Acta 51, 973-984.
111. Wronkiewicz, D.J. and Condie, K.C., 1987. Geochemistry of Archean shales from the Witwatersrand Supergroup, South Africa: Source-area weathering and provenance. Geochim. Cosmochim. Acta 51, 2401-2416.
112. Wronkiewicz, D.J. and Condie, K.C., 1989. Geochemistry and provenance of sediments from the Pongola Supergroup, South Africa: Evidence for a 3.0-Ga-old continental craton. Geochim. Cosmochim. Acta 53, 1537-1549.
113. Wronkiewicz, D.J. and Condie, K.C., 1990. Geochemistry and mineralogy of sediments from the Ventersdorp and Transvaal Supergroups, South Africa: Cratonic evolution during the early Proterozoic. Geochim. Cosmochim. Acta 54, 343-354.

FIGURE AND TABLE CAPTIONS

Figure 1: General geologic map of the Barberton greenstone belt with surrounding plutons. Insert shows Kaapvaal craton with location of the Barberton Greenstone Belt. Modified after Anhaeusser et al. (1983).

Figure 2: Pictures by Scanning Electron Microscopy of some minerals characteristic of the FTG shales (from A to F) and of the MG shales (G to L): A and B = flaky illite; C = dolomite and chlorite; D = monazite (rhabdophane); E = flaky chlorite; F = chlorite on quartz; G = flaky illite; H = vein filled with sphalerite; I = Cr-spinel; J = zircon; K = back-scattered image showing distribution of magnetite (white) in sample 79NC127; L = dolomite and quartz in a back-scattered image.

Figure 3: Logarithmic plots of TiO_2 (in A), Fe_2O_3 (in B) and K_2O (in C) vs. Al_2O_3. All contents are in wt%. Open circles are FTG shales and open squares MG shales. Adapted from Veizer and Garret (1978) and Veizer (1978). Mineral fields calculated from Deer et al. (1983).

Figure 4: K_2O-Fe_2O_3-Al_2O_3 ternary plot adapted from Wronkiewicz and Condie (1987). Field of residual clays is from Reimer (1985). The abbreviations stand for: FVO = felsic volcanic; KOM = komatiite; BAS = basalt; GRA = granite; TTG = tonalite/trondjhemite/granodiorite.

Figure 5: Ternary diagram of molar fractions of Al_2O_3-(CaO^*+Na_2O)-K_2O. Modified from Nesbitt and Young (1984) and McDaniel et al. (1994). Also plotted are the NASC (Gromet et

al., 1984) value (full square) and the upper continental crust (Taylor and McLennan, 1985) data (dashed area).

Figure 6: Logarithmic plot of Rb vs. K concentrations of the FTG and MG shales. Adapted from Veizer (1978). Mineral fields calculated from Deer et al. (1983).

Figure 7: Chondrite-normalized REE patterns of the FTG and MG shales as well as of the NASC reference.

Figure 8: Logarithmic plot of Cr vs. Ni concentrations of the FTG and MG shales relative to other Archaean shales of South Africa (in A) and to other early Archaean occurrences (in B). Data from Wronkiewicz and Condie (1987; 1989; 1990), McLennan et al. (1983a), McLennan et al. (1984), Nance and Taylor (1977) and Jenner et al. (1981).

Figure 9: Plot of Th/Sc vs. Zr/Sc ratios of the FTG and MG shales. Note positive correlation indicating simple compositional variation. Adapted from McLennan et al. (1993).

Figure 10: Plot of Cr vs. Zr contents of the FTG (circles) and MG (squares) shales. Note positive correlation in the Moodies shales.

Figure 11: Plot of Gd_N/Yb_N vs. La_N/Sm_N ratios. NASC ratios are for reference. The effects of heavy mineral sorting for apatite, monazite and zircon (- = loss, + = addition) are shown in insert. Adapted from Bock et al. (1994).

Figure 12: Double ternary diagram of Th-Hf-Co and La-Th-Sc contents, after Wronckiewicz and Condie (1987). Source rock compositions are Archaean (Condie, 1993) and NASC (Gromet et al., 1984). For abbreviations, see figure 4 and AS stands for Archean Shales (Condie, 1993).

Figure 13: Plot of Zr contents vs. Ti/Nb ratios (in A), and SiO_2 contents vs. Ti/Nb ratios (in B). Source rock compositions are Archaean (Condie, 1993) and NASC (Gromet et al., 1984). For the other abbreviations, see figure 4.

Figure 14: Plots of Th/Sc vs. Th/Al2O3 ratios (in A); Th/Al_2O_3 vs. Sc/Al_2O_3 ratios (in B); Th/Al_2O_3 vs. La/Al_2O_3 ratios (in C) and La/Sc vs. La_N/Yb_N ratios (in D). Adapted from Hemming et al. (1995). For abbreviations, see figure 4.

Figure 15: Pb-Pb isochron diagram for the FTG (circles) and MG (squares) shales.

Figure 16: Rb-Sr isochron diagram for the FTG (circles) and MG (squares) shales.

Figure 17: Diagram of $^{147}Sm/^{144}Nd$ vs. $^{143}Nd/^{144}Nd$ ratios of the FTG (circles) and MG (squares) shales.

Figure 18: TDM (Ga) vs. $^{147}Sm/^{144}Nd$ ratios. Data sources and identification: open circles are the FTG shales of our study and filled circles are the FTG shales (data of McCulloch and Wasserburg, 1978; Miller and O'Nions, 1985; Dia et al., 1990); open boxes are the MG shales of our study; open diamonds are felsic volcanics and granitoid rocks around the BGB (data of Hamilton et al., 1979; Kröner et al., 1996; Hegner, unpubl.); filled triangles are gneisses of the Ancient Gneiss Complex (data of Kröner et al., 1993); small open circles are komatiites (data of Hamilton et al., 1979; Jahn et al., 1982; Gruau et al., 1990; Lahaye et al., 1994; Lecuyer et al., 1994; Hegner, unpubl.); small filled circles are basaltic komatiites (data of Jahn et al., 1982; Lahaye et al., 1994; Lecuyer et al., 1994); open triangles are basalts (data of Hamilton et al., 1979; Jahn et al., 1982; Gruau et al., 1990). Age data are of Hamilton et al. (1979), Kröner et al. (1991) and Kröner et al. (1996).

Figure 19: ε_{Nd} vs. $^{147}Sm/^{144}Nd$ ratios at T = 3245 Ma of the FTG and MG shales, together with previously published isotopic values of FTG shales compared to possible source rocks. Symbols as in figure 18.

Figure 20: ε_{Nd} vs. time plot for Nd isotope data of the FTG shales. Notice that the evolution lines appear to converge at certain ages. The shaded boxes correspond to εNd data of known alteration ages of the area with Nd isotope data of the sampled shales (in Toulkeridis et al., 1998; Toulkeridis et al., 1999).

Table 1: Mineral composition, vein type and Chlorite/Illite (Chl/Ill) ratio of the FTG and MG shales. Abbreviations are: n.d. = not determined, Qz = quartz, Dol = dolomite, FeDol = Fe-dolomite, Ank = ankerite, Cc = calcite, Sid = siderite, Ill = illite, Chl = chlorite, Ba = barite, Apa = apatite, Mnz = monazite (rhabdophane), Illm = illmenite, Ti =

titanite/rutile, Mt = magnetite, Zr = zircon, CrSpi = Cr-spinel, Alb = albite, Kfsp = K-feldspar, PbS = galenite, Pyr = pyrite, ZnS, FeNiS, NiFeS, FeCuS, AsCoFeNiS = minor undifferentiated sulfides, FeTi and FeSi = undifferentiated Fe-bearing minerals.

Table 2a: Major, trace and rare-earth elements of the FTG shales. Major elements are in %wt, trace- and REE are in µg/g. Chemical data of 79NC117 and 79NC118 are from McLennan et al. (1983). Average* excludes 79NC107. For explanation see text.

Table 2b: Major-, trace and rare-earth elemenrs of the MG shales. Major elements are in %wt, trace- and REE are in µg/g. Chemical data of 79NC123, 79NC124, 79NC129, 79NC130 and 79NC131 are from McLennan et al. (1983). Average* excludes 79NC127. For explanation see text.

Table 3a: Selected elemental ratios of the FTG shales

Table 3b: Selected elemental ratios of the MG shales

Table 4: Rb, Sr, Sm, Nd concentrations and isotopic data of Sr, Pb and Nd in FTG and MG shales. N.d. = not determined.

For ε_{Nd} calculation the following equation was used:

$$\varepsilon_{Nd} = \left(\frac{(^{143}Nd/^{144}Nd)_{meas} - (^{147}Sm/^{144}Nd)_{meas} * (e^{\lambda T} - 1)}{0.512638 - 0.1966 * (e^{\lambda T} - 1)} - 1\right) * 10000$$

For T_{DM} calculation the following equation was used:

$$T_{DM} = \frac{1}{\lambda} * \ln\left(1 + \frac{0.513151 - (^{143}Nd/^{144}Nd)_{meas} - (e^{\lambda T} - 1) * ((^{147}Sm/^{144}Nd)_{meas} - 0.11)}{0.2137 - 0.11}\right)$$

Table 1

Sample	Mineralogy	Vein-type	Chl/Ill
79NC103	Qz-Ill-Chl-Dol		43
79NC104	Qz-Chl-Ill-Dol-Sid-Illm	Pyr	12.2
79NC105	Qz-Chl-Ill-Alb-Cc-Dol-Illm-Sid-Zr-Apa-Mt	Pyr-Au	19
79NC106	Qz-Chl-Ill-Dol-Zr-FeNiS	Qz	9.5
79NC107	Qz-Chl-Ill-(Ill-Chl)-Alb	Pyr-Au	11.3
79NC108	Qz-Chl-Ill-Alb-Dol	Pyr-Au	13.3
79NC111	Qz-Ill-Sid-Alb-Mnz		17.9
79NC113	Qz-Chl-Ill-(Ill-Chl)-Dol-FeCuS-FeTi-FeSi		12.5
79NC114	Qz-Ill-Chl-Illm-Dol-Mnz-Apa-FeSi	Dol-Qz	21.9
79NC115	Qz-Chl-Ill-(Ill-Chl)-FeCuS-FeNiS		16.8
79NC116	Qz-Chl-Ill-FeSi-Dol-Mnz	Dol	13.7
79NC117	Qz-Chl-(Ill-Chl)-Ill-Illm-Sid-Pyr-Mnz-FeSi-Alb?		17
79NC118	Qz-Chl-Alb-Sid-Pyr-Mnz-AsCoFeNiS-FeCuS-Ti		n.d.
79NC119	Qz-Chl-Ill-Alb-Illm-Dol	Dol-ZnS	9.1
79NC123	Qz-Ill-Chl-Dol-FeCuS-Mnz		n.d.
79NC124	Qz-Ill-(Ill-Chl)-Chl-Dol-Sid-Illm-Alb-Zr-Ti-FeSi-ZnS-Mnz?		n.d.
79NC125	Qz-Ill-Alb-Chl-Illm-Dol-FeNiS-Zr-Pyr		100
79NC126	Qz-Ill-(Ill-Chl)-Alb-CrSpi-Dol-Mnz-FeNiS-AsCoFeNiS-FeCuS		100
79NC127	Qz-Mt-(Ill-Chl)-Ill-Alb-Chl-Mnz-FeSi-Pyr	Qz	41
79NC128	Qz-Ill-Alb-Dol-FeSi-FeNiS-Ti		82
79NC129	Qz-Chl-Ill-Alb-Pyr-Illm		8.5
79NC130	Qz-Ill-Chl-Alb-Pyr-Mnz-CrSpi-Ti	Dol	n.d.
79NC131	Qz-Ill-Chl-Sid-Alb-Mnz-NiFeS-Ba-Illm-Ti		n.d.

Table 2a

Elements	79NC 103	79NC 104	79NC 105	79NC 106	79NC 107	79NC 108	79NC 111	79NC 113	79NC 114	79NC 115	79NC 116	79NC 117	79NC 118	79NC 119	AVG	AVG*
SiO_2	50.73	51.12	52.03	55.64	73.88	55.29	53.91	54.79	56.14	57.51	53.33	50.16	58.86	57.72	55.79	54.40
TiO_2	0.74	0.62	0.62	0.71	0.31	0.61	0.65	0.63	0.60	0.71	0.67	0.69	0.52	0.70	0.61	0.64
Al_2O_3	14.76	14.36	11.76	13.22	8.24	11.65	12.63	12.32	13.81	13.55	13.24	17.40	13.05	14.16	13.15	13.53
Fe_2O_3T	9.58	12.27	8.55	10.26	6.77	8.77	9.30	10.37	8.04	7.50	10.95	10.69	9.57	9.26	9.42	9.62
MnO	0.14	0.13	0.31	0.13	0.05	0.20	0.22	0.17	0.14	0.15	0.14	0.11	0.08	0.10	0.15	0.16
MgO	6.13	8.07	6.02	7.35	4.67	6.80	6.27	7.49	6.41	5.52	7.76	6.81	7.06	7.01	6.67	6.82
CaO	1.78	0.51	5.53	2.12	0.50	3.76	3.97	2.05	1.81	2.56	1.38	0.30	0.48	1.16	1.99	2.11
Na_2O	0.36	1.25	1.30	1.48	0.33	1.38	1.20	1.10	1.76	1.93	1.24	0.80	1.09	2.05	1.23	1.30
K_2O	4.22	2.13	2.34	1.44	1.22	1.78	2.19	1.70	2.54	2.33	1.85	3.37	1.78	1.53	2.17	2.25
P_2O_5	0.13	0.11	0.11	0.13	0.07	0.11	0.12	0.10	0.10	0.12	0.11	0.11	0.11	0.12	0.11	0.11
L.O.I.	11.17	9.21	11.59	7.50	4.76	10.07	9.95	9.45	9.42	8.19	9.38	9.67	7.52	6.69	8.90	9.22
Total	99.75	99.78	100.16	99.97	100.80	100.42	100.41	100.17	100.77	100.08	100.05	100.11	100.12	100.50	100.21	100.16
CIA	64.60	74.10	44.80	63.70	76.00	52.00	52.80	63.30	61.40	57.40	67.80	76.80	75.10	67.40	64.08	63.17
CIW	80.80	84.10	49.60	68.90	86.50	56.80	58.60	69.90	69.90	64.20	75.50	91.60	84.50	73.20	72.44	71.36
Cs	4.89	1.96	2.23	1.71	1.56	1.61	2.19	2.36	3.25	2.33	1.46	7.41	3.44	2.45	2.78	2.87
Ba‡	517.00	409.00	306.00	235.00	203.00	256.00	298.00	247.00	427.00	392.00	325.00	588.00	246.00	276.00	337.50	347.85
Ba	454.00	409.00	291.00	237.00	208.00	253.00	312.00	216.00	452.00	401.00	322.00	588.00	246.00	294.00	334.50	344.23
Pb	5.50	6.00	6.10	5.00	9.20	4.80	4.00	3.60	5.00	4.00	4.00	3.70	2.60	9.00	5.18	4.87
La	25.03	32.24	18.29	19.31	18.82	19.24	21.96	16.41	20.62	26.68	24.69	24.80	16.30	23.20	21.97	22.21
Ce	48.02	58.82	37.40	37.87	36.12	36.98	38.59	31.48	39.47	52.28	44.52	53.80	37.50	44.30	42.65	43.16
Pr	5.40	6.46	4.22	4.29	3.93	4.22	4.54	3.55	4.56	5.81	5.18	6.51	4.20	5.17	4.86	4.93
Nd	24.56	28.62	19.25	19.67	17.32	19.21	20.62	15.97	20.40	25.10	22.45	24.70	16.80	23.02	21.26	21.57
Sm	4.58	5.94	4.05	4.08	3.06	3.83	4.07	3.42	4.33	5.50	4.33	4.79	3.28	4.84	4.29	4.39
Eu	1.41	1.57	1.28	1.22	0.79	1.14	1.18	0.95	1.35	1.43	1.21	1.22	0.88	1.38	1.22	1.25
Gd	3.86	4.60	3.65	3.43	2.44	3.29	3.79	2.74	3.60	4.34	3.94	4.02	2.86	4.11	3.62	3.71
Tb	0.75	0.84	0.71	0.64	0.44	0.57	0.73	0.54	0.65	0.76	0.75	0.70	0.48	0.75	0.67	0.68
Dy	4.39	4.79	4.74	4.15	2.50	3.86	4.43	3.46	4.25	5.04	4.93	3.96	3.19	4.97	4.19	4.32
Ho	0.88	0.94	0.92	0.84	0.52	0.78	0.94	0.68	0.85	1.00	0.96	0.88	0.78	0.99	0.85	0.88
Er	2.51	2.74	2.61	2.48	1.50	2.15	2.66	2.02	2.42	2.88	2.75	2.48	2.07	2.67	2.42	2.50
Tm	0.36	0.39	0.39	0.35	0.21	0.32	0.38	0.31	0.36	0.44	0.41			0.40	0.36	0.37

Table 2a (continued)

Elements	79NC 103	79NC 104	79NC 105	79NC 106	79NC 107	79NC 108	79NC 111	79NC 113	79NC 114	79NC 115	79NC 116	79NC 117	79NC 118	79NC 119	AVG	AVG*
Yb	2.34	2.48	2.45	2.24	1.36	1.99	2.44	1.83	2.19	2.52	2.40	2.33	2.00	2.39	2.21	2.28
Lu	0.37	0.40	0.40	0.38	0.26	0.32	0.43	0.31	0.36	0.45	0.44			0.44	0.38	0.39
Y‡	27.00	25.00	26.00	22.00	13.00	20.00	23.00	22.00	21.00	23.00	22.00	28.00	21.00	23.00	22.57	23.31
Y	22.00	25.00	25.00	22.00	14.00	20.00	24.00	19.00	22.00	26.00	24.00	28.00	21.00	25.00	22.69	23.36
Th‡	4.50	4.40	4.80	5.70	4.50	4.20	4.20	4.00	3.90	5.00	4.60	5.50	4.20	4.20	4.55	4.55
Th	5.00	5.00	5.30	5.50	4.50	4.50	5.40	3.60	4.50	5.50	4.60	5.50	4.20	5.50	4.89	4.92
U	1.60	1.40	1.70	1.50	1.50	1.40	1.70	1.10	1.40	1.80	1.40	1.70	1.20	1.60	1.50	1.50
Zr	102.00	89.00	109.00	113.00	63.00	101.00	103.00	96.00	88.00	113.00	98.00	127.00	121.00	107.00	102.14	105.15
Hf	3.99	3.48	3.79	4.02	2.30	3.41	3.56	2.68	3.11	4.34	2.96	3.66	2.67	3.49	3.39	3.47
Ta	1.07	1.21	1.09	1.13	1.14	0.99	0.11	0.05	0.92	1.34	0.11			0.04	0.77	0.73
Nb	8.00	7.00	6.00	8.00	5.00	5.00	7.00	8.00	6.00	9.00	7.00	13.00	10.00	7.00	7.52	7.72
Mo	2.13	2.02	1.49	1.84	1.28	1.67	2.23	0.51	2.50	3.19	1.06	1.33	1.26	1.45	1.71	1.74
Cr	1027.00	1023.00	977.00	1029.00	393.00	888.00	969.00	1006.00	996.00	986.00	1029.00	1120.00	854.00	952.00	946.36	988.92
V	192.00	177.00	156.00	160.00	73.00	142.00	162.00	162.00	170.00	168.00	166.00	194.00	144.00	167.00	159.50	166.15
Sc	28.00	26.00	22.00	24.00	14.00	23.00	29.00	24.00	26.00	25.00	24.00	28.00	22.00	26.00	24.38	25.15
Ni‡	353.00	395.00	316.00	434.00	193.00	346.00	384.00	424.00	370.00	306.00	381.00	526.00	555.00	430.00	386.64	401.54
Ni	440.00	535.00	381.00	507.00	241.00	408.00	457.00	401.00	487.00	397.00	487.00	526.00	555.00	500.00	451.57	467.77
Co	80.00	69.00	59.00	89.00	87.00	74.00	77.00	88.00	87.00	66.00	64.00	46.00	38.00	45.00	69.21	67.85
Cu	53.00	28.00	46.00	54.00	27.00	54.00	57.00	45.00	51.00	42.00	60.00	115.00	78.00	65.00	55.36	57.54
Ga	19.80	18.10	13.50	15.50	10.70	14.00	15.90	15.30	16.90	16.00	16.30	24.00	16.00	17.20	16.37	16.81
Zn	146.00	120.00	92.00	125.00	86.00	98.00	112.00	122.00	96.00	42.00	164.00			143.00	112.17	114.55
Rb	131.00	70.00	83.00	55.00	57.00	59.00	86.00	54.00	98.00	84.00	52.00			64.00	74.52	76.09
Sr	88.00	21.00	112.00	60.00	19.00	101.00	93.00	38.00	62.00	80.00	37.00			46.00	63.04	67.08
Li	45.90	101.00	46.40	95.90	85.30	59.90	64.40	95.50	78.10	71.50	88.40			112.00	78.69	78.09
Be	1.81	1.71	1.34	1.29	0.99	1.21	1.44	1.05	1.81	1.76	1.26			1.59	1.44	1.48

Table 2b

Elements	79NC 123	79NC 124	79NC 125	79NC 126	79NC 127	79NC 128	79NC 129	79NC 130	79NC 131	AVG	AVG*
SiO_2	61.93	59.44	61.01	63.09	40.21	62.17	58.12	61.59	55.53	58.12	60.36
TiO_2	0.36	0.38	0.50	0.52	0.34	0.43	0.55	0.47	0.43	0.44	0.46
Al_2O_3	11.07	13.30	12.98	13.56	7.72	12.02	15.37	14.86	15.04	12.88	13.53
Fe_2O_3T	7.79	6.01	5.50	4.60	38.13	6.04	9.21	6.46	7.34	6.71	4.81
MnO	0.14	0.14	0.09	0.07	0.25	0.08	0.11	0.09	0.15	0.12	0.11
MgO	5.19	4.97	3.92	3.13	3.63	3.53	5.45	4.78	5.07	4.41	4.51
CaO	2.59	1.92	1.11	0.84	0.49	1.14	0.58	0.87	0.80	1.15	1.23
Na_2O	0.96	2.07	1.68	1.97	2.33	1.71	2.03	2.21	1.52	1.83	1.77
K_2O	3.59	4.62	4.77	5.53	1.91	4.49	4.71	5.94	5.49	4.56	4.89
P_2O_5	0.08	0.08	0.07	0.09	0.09	0.07	0.08	0.08	0.08	0.08	0.08
L.O.I.	6.36	7.18	8.87	6.99	4.83	8.25	3.89	2.74	8.61	6.41	6.61
Total	99.98	100.03	100.50	100.39	99.92	99.94	100.02	100.01	99.98	100.08	100.11
CIA	52.60	53.20	57.00	56.30	54.00	55.70	62.30	56.50	60.80	56.48	56.78
CIW	64.50	66.50	73.80	74.90	63.10	71.80	78.50	74.70	80.00	71.98	73.08
Cs	2.23	4.03	3.39	5.87	11.40	3.71	3.81	20.20	6.55	6.80	6.22
Baţ	345.00	547.00	668.00	510.00	246.00	516.00	606.00	718.00	458.00	512.67	546.00
Ba			526.00	507.00	212.00	519.00					
Pb	4.80	9.70	7.60	8.80	5.70	8.10	9.60	8.10	5.90	7.58	7.82
La	14.50	16.70	24.90	19.16	14.12	17.19	34.60	18.40	26.70	20.70	21.52
Ce	28.90	35.70	42.84	34.36	26.74	32.38	70.30	37.80	54.80	40.42	42.14
Pr	3.45	3.77	4.43	4.04	3.04	3.49	7.28	4.34	6.38	4.47	4.65
Nd	13.20	14.70	19.00	15.89	12.66	15.21	28.90	17.00	24.30	17.87	18.53
Sm	2.39	2.73	3.22	2.79	2.51	2.84	5.28	3.01	4.64	3.27	3.36
Eu	0.68	0.73	1.03	0.88	0.83	0.94	1.27	0.80	1.30	0.94	0.95
Gd	2.07	2.14	2.65	2.79	2.27	2.32	3.61	2.38	3.94	2.69	2.74
Tb	0.36	0.37	0.43	0.44	0.42	0.38	0.56	0.42	0.61	0.44	0.45
Dy	2.08	2.18	2.63	2.73	2.70	2.47	3.30	2.42	3.53	2.67	2.67
Ho	0.49	0.50	0.46	0.58	0.51	0.49	0.77	0.55	0.79	0.57	0.58
Er	1.39	1.57	1.31	1.72	1.43	1.29	2.26	1.60	2.22	1.64	1.67
Tm			0.20	0.31	0.22	0.24				0.24	0.25

Table 2b (continued)

Elements	79NC 123	79NC 124	79NC 125	79NC 126	79NC 127	79NC 128	79NC 129	79NC 130	79NC 131	AVG	AVG*
Yb	1.29	1.38	1.20	1.65	1.44	1.36	2.04	1.63	2.13	1.57	1.59
Lu			0.22	0.26	0.24	0.22				0.24	0.23
Y‡	15.30	20.70	17.00	16.00	29.00	15.00	26.30	22.10	23.10	20.50	19.44
Y				15.80							
Th‡	5.30	5.20	5.90	6.60	2.50	3.80	7.10	6.20	7.20	5.53	5.91
Th			5.20	6.70	3.70	5.00					
U	1.60	1.50	1.60	2.20	1.30	1.90	2.40	1.90	2.30		
Zr	115.00	131.00	128.00	170.00	82.00	115.00	209.00	109.00	175.00	137.11	144.00
Hf	3.40	3.10	3.09	5.51	3.01	5.07	4.43	5.06	5.52	4.24	4.40
Ta	n.d.	n.d.	0.16	1.38	0.62	0.39	n.d.	n.d.	n.d.	0.64	0.64
Nb	9.80	10.10	8.00	10.00	6.00	7.00	13.70	10.90	10.70	9.57	10.02
Mo	0.82	0.99	1.42	1.33	1.34	6.31	1.29	1.41	1.46	1.82	1.88
Cr	643.00	577.00	677.00	717.00	535.00	509.00	822.00	679.00	855.00	668.20	684.90
V	65.00	91.00	90.00	85.00	105.00	81.00	124.00	100.00	109.00	94.44	93.13
Sc	14.00	15.00	14.70	11.50	16.40	13.80	18.00	15.00	15.00	14.82	14.63
Ni‡	287.00	287.00	194.00	134.00	162.00	213.00	394.00	323.00	366.00	262.20	274.80
Ni			194.00	154.00	162.00	213.00					
Co	30.00	36.00	106.00	98.00	179.00	131.00	39.00	35.00	36.00	76.67	63.88
Cu	37.00	3.30	8.00	39.00	33.00	54.00	3.00	68.00	25.00	30.03	29.66
Ga	11.00	13.00	16.90	16.70	10.10	15.70	13.00	16.00	14.00	14.04	14.54
Zn			101.00	43.00	53.00	36.00				58.25	60.00
Rb			107.00	139.00	85.80	126.00					
Sr			104.00	76.73	41.50	122.00					
Li			31.90	24.91	32.10	23.40				28.08	26.74
Be			1.89	1.93	1.15	2.09				1.77	1.97

Table 3a

Elements	79NC 103	79NC 104	79NC 105	79NC 106	79NC 107	79NC 108	79NC 111	79NC 113	79NC 114	79NC 115	79NC 116	79NC 117	79NC 118	79NC 119	AVG	AVG*
SiO_2/Al_2O_3	3.44	3.56	4.42	4.21	8.97	4.75	4.27	4.45	4.07	4.24	4.03	2.88	4.51	4.08	4.42	4.07
K_2O/Na_2O	11.72	1.70	1.80	0.97	3.70	1.29	1.83	1.55	1.44	1.21	1.49	4.21	1.63	0.75	2.52	2.43
Th/U	3.06	3.55	3.06	3.70	2.94	3.23	3.12	3.34	3.10	3.07	3.27	3.26	3.51	3.50	3.27	3.29
Th/Sc	0.16	0.17	0.21	0.24	0.31	0.18	0.14	0.17	0.15	0.20	0.19	0.19	0.19	0.16	0.19	0.18
Zr/Hf	25.56	25.57	28.76	28.11	27.39	29.62	28.93	35.82	28.30	26.04	33.11	34.70	45.32	30.66	30.56	30.81
Zr/Nb	12.75	12.71	18.17	14.13	12.60	20.20	14.71	12.00	14.67	12.56	14.00	10.16	12.31	15.29	14.02	14.13
Zr/Y	3.78	3.56	4.19	5.14	4.85	5.05	4.48	4.36	4.19	4.91	4.45	4.58	5.68	4.65	4.56	4.54
Ti/Zr	43.49	41.76	34.10	37.67	29.50	36.21	37.83	39.34	40.88	37.67	40.99	23.13	25.76	39.22	35.97	36.27
Ti/Nb	554.50	531.00	619.50	532.10	371.70	731.40	556.70	472.10	599.50	472.90	573.80	235.00	317.10	599.50	488.30	494.20
Cr/Zr	10.07	11.49	8.96	9.11	6.24	8.79	9.41	10.48	11.32	8.73	10.50	8.82	7.06	8.90	9.28	9.51
Cr/V	5.35	5.78	6.26	6.43	5.38	6.25	5.98	6.21	5.86	5.87	6.20	5.77	5.93	5.70	5.93	5.97
V/Ni	0.54	0.45	0.49	0.37	0.38	0.41	0.42	0.38	0.46	0.55	0.44	0.37	0.26	0.39	0.42	0.43
Ni/Co	4.41	5.72	5.36	4.88	2.22	4.68	4.99	4.82	4.25	4.64	5.95	11.43	14.61	9.56	6.25	6.56
La/Th	5.56	7.33	3.81	3.39	4.18	4.58	5.23	4.10	5.29	5.34	5.37	4.60	3.90	5.52	4.87	4.92
La/Sc	0.88	1.26	0.81	0.82	1.31	0.82	0.75	0.70	0.79	1.09	1.02	0.89	0.74	0.90	0.91	0.88
La/Yb	10.70	13.00	7.47	8.62	13.84	9.67	9.00	8.97	9.42	10.59	10.29	10.60	8.20	9.71	10.00	9.71
La_N/Yb_N	7.15	8.69	4.99	5.76	9.25	6.47	6.02	6.00	6.30	7.08	6.88	7.12	5.45	6.49	6.64	6.52
Eu/Eu*	0.92	0.82	0.93	0.91	0.80	0.91	0.85	0.84	0.96	0.81	0.83	0.79	0.83	0.87	0.86	0.86
ΣREE	124.46	150.83	100.36	100.95	89.27	97.90	106.76	83.67	105.41	134.23	118.96	130.90	90.90	118.63	110.95	112.61

Table 3b

Elements	79NC 123	79NC 124	79NC 125	79NC 126	79NC 127	79NC 128	79NC 129	79NC 130	79NC 131	AVG	AVG*
SiO_2/Al_2O_3	5.59	4.47	4.70	4.65	5.21	5.17	3.78	4.14	3.69	4.60	4.53
K_2O/Na_2O	3.74	2.23	2.84	2.81	0.82	2.63	2.32	2.69	3.61	2.63	2.86
Th/U	3.31	3.47	3.69	2.00	1.92	2.00	2.96	3.26	3.13	6.19	6.73
Th/Sc	0.38	0.35	0.40	0.57	0.15	0.28	0.39	0.41	0.48	0.38	0.41
Zr/Hf	33.80	42.30	41.42	30.85	27.24	22.68	47.20	21.50	31.70	33.19	33.93
Zr/Nb	11.79	12.97	16.00	17.00	13.67	16.43	15.26	10.00	16.36	14.39	14.48
Zr/Y	7.52	6.33	7.53	10.63	2.83	7.67	7.95	4.93	7.58	6.99	7.52
Ti/Zr	18.77	17.39	23.42	18.34	24.86	22.42	15.78	25.85	14.73	19.34	18.94
Ti/Nb	221.40	225.60	374.70	311.70	339.70	368.30	240.70	258.50	240.90	277.00	272.30
Cr/Zr	5.59	4.40	5.29	4.22	6.52	4.43	3.93	6.23	4.89	5.06	4.87
Cr/V	9.89	6.34	7.52	8.44	5.10	6.28	6.63	6.79	7.84	7.20	7.47
V/Ni	0.23	0.32	0.46	0.63	0.65	0.38	0.31	0.31	0.30	0.40	0.37
Ni/Co	9.57	7.97	1.83	1.37	0.91	1.63	10.10	9.23	10.17	5.86	6.48
La/Th	2.70	3.20	4.22	2.90	5.65	4.52	4.90	3.00	3.70	3.87	3.64
La/Sc	1.00	1.10	1.69	1.67	0.86	1.25	1.90	1.20	1.80	1.39	1.45
La/Yb	11.20	12.10	20.75	11.61	9.81	12.64	17.00	11.30	12.50	13.21	13.64
La_N/Yb_N	7.52	8.09	13.88	7.76	6.56	8.45	11.34	7.55	8.38	8.82	9.08
Eu/Eu*	0.87	0.84	1.01	0.96	0.99	1.04	0.79	0.83	0.88	0.91	0.90
ΣREE	71.20	82.47	104.52	87.60	69.13	80.82	160.80	90.80	132.00	97.70	101.30

Table 4

Sample	Rb	Sr	$^{87}Rb/^{86}Sr$	$^{87}Sr/^{86}Sr$	Sm	Nd	$^{147}Sm/^{144}Nd$	fSm/Nd	$^{143}Nd/^{144}Nd$	$\varepsilon_{Nd}(0)$	$\varepsilon_{Nd}(T)$	T_{DM} (Ga)	$^{206}Pb/^{204}Pb$	$^{207}Pb/^{204}Pb$	$^{208}Pb/^{204}Pb$
79NC103	147	86	5.0438	0.910879	4.58	24.56	0.1128	-0.4262	0.511042	-31.13	3.96	3.17	25.699	17.155	46.885
79NC104	71	21	10.1751	1.118376	5.94	28.62	0.1255	-0.3614	0.510893	-34.04	-4.35	3.77	25.901	17.142	50.472
79NC105	91	112	2.374	0.80864	4.05	19.25	0.1273	-0.3527	0.511226	-27.54	1.48	3.35	n.d.	n.d.	n.d.
79NC106	57	60	2.7809	0.827727	4.08	19.67	0.1255	-0.3618	0.511072	-30.55	-0.79	3.51	29.331	17.587	50.225
79NC107	59	19	9.339	1.111096	3.06	17.32	0.1069	-0.4564	0.510752	-36.79	0.76	3.4	19.362	15.881	38.209
79NC108	66	103	1.868	0.78507	3.83	19.21	0.1206	-0.3866	0.511139	-29.24	2.58	3.27	22.128	16.46	42.329
79NC111	84	85	2.8942	0.832729	4.07	20.62	0.1194	-0.3927	0.511096	-30.08	2.24	3.29	n.d.	n.d.	n.d.
79NC113	65	43	4.4577	0.904182	3.42	15.97	0.1295	-0.3411	0.511053	-30.92	-2.88	3.67	27.177	17.209	48.443
79NC114	97	59	4.8541	0.916865	4.33	20.4	0.1284	-0.3469	0.511044	-31.09	-2.58	3.64	23.598	16.749	41.465
79NC115	83	74	3.2892	0.846386	5.5	25.1	0.1325	-0.3258	0.510992	-32.11	-5.35	3.85	35.619	18.755	59.934
79NC116	65	37	5.1707	0.884431	4.33	22.45	0.1167	-0.4066	0.51094	-33.12	0.32	3.43	n.d.	n.d.	n.d.
79NC117	152	30	15.2486	1.086297	4.79	24.7	0.1173	-0.4034	0.511029	-31.39	1.81	3.32	36.807	19.01	64.418
79NC118	108	26	12.6016	1.250059	3.28	16.8	0.1181	-0.3993	0.511073	-30.53	2.33	3.28	34.75	18.653	64.317
79NC119	64	44	4.2854	0.89452	4.84	23.02	0.1272	-0.3531	0.511277	-26.55	2.52	3.27	n.d.	n.d.	n.d.
79NC123	91	75	3.5755	0.832605	2.39	13.2	0.1095	-0.443	0.511071	-30.57	4.84	3.02	31.007	17.875	49.622
79NC124	110	76	4.2364	0.820973	2.73	14.7	0.1123	-0.4288	0.51098	-32.34	1.9	3.24	23.306	16.893	41.439
79NC125	136	116	3.4398	0.851264	3.22	19	0.1025	-0.4786	0.510673	-38.33	-0.12	3.39	22.294	16.579	43.969
79NC126	142	87	4.8156	0.909332	2.79	15.89	0.1062	-0.4598	0.510829	-35.29	1.43	3.27	23.943	16.948	43.476
79NC127	103	48	6.3419	0.927248	2.51	12.66	0.1199	-0.3901	0.511037	-31.23	-0.09	3.38	n.d.	n.d.	n.d.
79NC128	127	115	3.2361	0.838492	2.84	15.21	0.1129	-0.4257	0.510736	-37.1	-3.14	3.61	n.d.	n.d.	n.d.
79NC129	180	110	4.7636	0.829305	5.28	28.9	0.1105	-0.4379	0.510833	-35.21	-0.25	3.4	25.914	17.693	44.813
79NC130	103	189	1.6013	0.800471	3.01	17	0.1071	-0.4552	0.51084	-35.07	1.28	3.28	28.399	17.72	47.324
79NC131	271	206	3.847	0.787697	4.64	24.3	0.1155	-0.4125	0.510933	-33.26	-0.33	3.4	29.681	17.561	50.092